

**Rosal Rubio Manuela**

**De:** Javier Gilabert <javier.gilabert@upct.es>  
**Enviado el:** domingo, 17 de mayo de 2015 18:44  
**Para:** Participación Pública  
**Asunto:** Aguas costeras  
**Datos adjuntos:** 2015 Baudron et al Journal of Hydrology.pdf

Apreciado Jesús,

Tal y como comenté en la reunión mantenida en la mesa sectorial de aguas costeras te adjunto un trabajo que acabamos de publicar en Journal of Hydrology sobre la entrada de aguas subterráneas al Mar Menor. El estudio se basa en una serie de campañas de medida de radioisótopos combinada con una modelización de la aportaciones por la rambla del Albujón y de ciclos de medidas in situ de una serie de 24 horas solapadas con medidas de correntómetros en la zona. Se hace referencia a la estimación de los 5 Hm3 y se corrige por el efecto de los gradientes de presión horizontal debido fundamentalmente a las mareas. La semana que viene aportaré algunos comentarios adicionales a la reunión mantenida.

Un saludo

Javier Gilabert

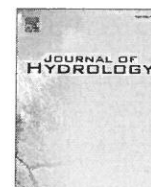
---

Department of Chemical & Environmental Engineering  
 Underwater Vehicles Lab (LVS)  
 Universidad Politécnica de Cartagena (UPCT)  
 Alfonso XIII, 52, E-30203, Cartagena, Spain  
 Tel.: +34 968 325 669

---

REGISTRACIÓN HIDROGRÁFICA DEL SEGURO	
SECCION DE PLANIFICACION HIDROLOGICA	
ENTRADA	FECHA 19 MAYO 2015
	Nº 212/2015
PASE	COPIA <input type="checkbox"/> A
	ORIGINAL <input type="checkbox"/>
Aprobación P.H.C.	
<input type="checkbox"/>	Para informe
<input type="checkbox"/>	Para conocimiento
<input type="checkbox"/>	Para despachar conmigo
<input type="checkbox"/>	Preparar contestación





# Combining radon, short-lived radium isotopes and hydrodynamic modeling to assess submarine groundwater discharge from an anthropized semiarid watershed to a Mediterranean lagoon (Mar Menor, SE Spain)



Paul Baudron<sup>a,b,h,i,\*</sup>, Sabine Cockenpot<sup>c</sup>, Francisco Lopez-Castejon<sup>d</sup>, Olivier Radakovitch<sup>c</sup>, Javier Gilabert<sup>d</sup>, Adriano Mayer<sup>e</sup>, José Luis Garcia-Arostegui<sup>f,g</sup>, David Martinez-Vicente<sup>a,g</sup>, Christian Leduc<sup>b</sup>, Christelle Claude<sup>c</sup>

<sup>a</sup> Fundación Instituto Euromediterráneo del Agua, Complejo Campus de Espinardo, Ctra. N301, 30100 Espinardo (Murcia), Spain

<sup>b</sup> Institut pour la Recherche et le Développement, UMR G-EAU, Cemagref, 361 rue Jean-François Breton, BP 5095, 34196 Montpellier Cedex 5, France

<sup>c</sup> CEREGE, Aix Marseille University, CNRS – UMR7330, BP 80, 13545 Aix-en-Provence, France

<sup>d</sup> Department of Chemical & Environmental Engineering, Universidad Politécnica de Cartagena (UPCT), Alfonso XIII, 54, E-30203 Cartagena, Spain

<sup>e</sup> EMMAH-UMR 1114, Université d'Avignon et des Pays de Vaucluse, 33 rue Louis Pasteur, 84000 Avignon, France

<sup>f</sup> Geological Survey of Spain (IGME), Avda. Miguel de Cervantes, 45 – 5° A, 30009 Murcia (Murcia), Spain

<sup>g</sup> University of Murcia, Institute for Water and Environment (INUAMA), Campus de Espinardo, 30100 Murcia, Spain

<sup>h</sup> Department of Civil, Geological and Mining Engineering, École Polytechnique de Montréal, C.P. 6079 Succ. Centre-Ville, Montréal, Québec H3C 3A7, Canada

<sup>i</sup> Geotop Research Center, Canada

## ARTICLE INFO

### Article history:

Received 20 June 2014

Received in revised form 13 January 2015

Accepted 5 March 2015

Available online 14 March 2015

This manuscript was handled by Laurent Charlet, Editor-in-Chief, with the assistance of Philippe Negrel, Associate Editor

### Keywords:

Submarine groundwater discharge

Radon

Radium

Hydrodynamic modeling

Nitrate

Reverse osmosis desalination

## SUMMARY

In highly anthropized watersheds, surface water tributaries may carry unexpected high quantities of radon and radium to coastal lagoons. Investigating submarine groundwater discharge (SGD) with radionuclide tracers is therefore a complex task. In order to quantify SGD and decipher the influence of the different water sources, we combined a radon ( $^{222}\text{Rn}$ ) and short-lived radium ( $^{223}\text{Ra}$ ,  $^{224}\text{Ra}$ ) survey with the hydrodynamic modeling of a lagoon. We applied it to the Mar Menor lagoon (SE Spain) where surface water tributaries and undocumented emissaries carry water from groundwater drainage and brines from groundwater desalination. We identified the areas of influence of the plume of radionuclides from the river, located major areas of SGD and proposed a location for two submarine emissaries. Porewater, i.e. interstitial water from underlying sediments, was found to be the most representative SGD end member, compared to continental groundwater collected from piezometers. Mass balances in winter and summer seasons provided yearly SGD fluxes of water of  $0.4\text{--}2.2 \cdot 10^8 \text{ m}^3/\text{y}$  ( $^{222}\text{Rn}$ ),  $4.4\text{--}19.0 \cdot 10^8 \text{ m}^3/\text{y}$  ( $^{224}\text{Ra}$ ) and  $1.3 \cdot 10^8 \text{ m}^3/\text{y}$  ( $^{223}\text{Ra}$ , measured in winter only). Tidal pumping was identified as a main driver for recirculated saline groundwater, while fresh submarine groundwater discharge from the aquifer ranged between 2% and 23% of total SGD.

© 2015 Elsevier B.V. All rights reserved.

## 1. Introduction

Increasing anthropogenic pressure might affect the hydrology and ecology of coastal areas by modifying submarine groundwater

discharge (SGD) (e.g. Burnett et al., 2003). In the Mediterranean Sea, such processes are a particular source of concern in wetlands (e.g. Rodellas et al., 2012), lagoons (e.g. Gattacceca et al., 2011) and coastal areas (e.g. Schiavo et al., 2009). SGD assessment is therefore a critical need for water resources management, although groundwater inputs into surface water masses are difficult to quantify.

In this context, approaches based on radon and radium contents may be very efficient. They rely on a global mass balance, as pioneered by Moore (1996) or Cable et al. (1996). Their interest is a simple field implementation and a spatio-temporal integration. Over the last decade, numerous authors successfully applied this method in many places worldwide (e.g. Burnett et al., 2008;

\* Corresponding author at: Department of Civil, Geological and Mining Engineering, École Polytechnique de Montréal, C.P. 6079 Succ. Centre-Ville, Montréal, Québec H3C 3A7, Canada. Tel.: +1 514 431 2740.

E-mail addresses: paul.baudron@baudron.com (P. Baudron), sabine.cockenpot@gmail.com (S. Cockenpot), francisco.lopez@upct.es (F. Lopez-Castejon), radakovitch@cerege.fr (O. Radakovitch), javier.gilabert@upct.es (J. Gilabert), adriano.mayer@univ-avignon.fr (A. Mayer), jarostegui@igme.es (J.L. Garcia-Arostegui), davidmv@um.es (D. Martinez-Vicente), christian.leduc@ird.fr (C. Leduc), claude@cerege.fr (C. Claude).

Cook et al., 2008; Loveless et al., 2008; Mulligan and Charette, 2006; Santos et al., 2008; Santos and Eyre, 2011) and to a lesser extent in the Mediterranean (e.g. García-Solsona et al., 2010; Gattacceca et al., 2011; Rodellas et al., 2012; Weinstein et al., 2007).

The most delicate part of the mass balance method relies on a precise determination of the discharge rates and the radionuclide activities of the different terms of the mass balance. Such calculation is particularly sensitive to the composition of discharging groundwater and to the assessment of inputs from surface water.

The behavior of radon and radium in coastal aquifers is complex (e.g. Burnett et al., 2003). Some authors tried to explain the origin of this variability (e.g. Dulaiova et al., 2008; Gonneea et al., 2008), but general guidelines are difficult to draw. Radon and radium are brought to coastal environments by terrestrial water carried by the regional subterranean hydrodynamics, but also by the recirculation of saline water in the sediments (e.g. Taniguchi et al., 2006; Gattacceca et al., 2011). These two processes bring two distinct components of SGD that are designated, in most studies, as fresh submarine groundwater discharge (FSGD) and "Recirculated Saline Groundwater Discharge" (RSGD).

FSGD corresponds to the discharge of continental groundwater into surface water masses, thus affecting the water balance of the aquifer system. It is mainly driven by terrestrial hydraulic gradients and tidal pumping. Continental groundwater can be defined as "deeper and fresher" water (Cyronak et al., 2013) than seawater. Still, they might in some cases reach levels of salinities similar to that of seawater. RSGD is the result of a series of mechanisms that force seawater to flow across the sediment–water interface, mix with porewater (i.e. shallow interstitial water from sediments underlying the water mass) and continental groundwater if present and discharge back into surface water masses. It does not affect the water balances of the aquifer and surface water, but modifies significantly radon and radium mass balances. The driving forces of both recirculated and continental groundwater discharge were reviewed by Santos et al. (2012) and may include additional advective processes like wave setup, wave pumping, ripple migration, bioturbation or gas bubble upwelling.

By contrast to SGD, surface water fluxes often represent limited inputs of radionuclides. Nonetheless, when rivers drain aquifers or are fed by additional source of radionuclides, they may provide important quantities of radionuclides to coastal systems (Gattacceca et al., 2011). Their influence on the tracer distribution and on the radionuclide mass balance is hard to assess. Very reactive surface-water hydrodynamics even complicates this task by inducing a fast dispersion of the tracers due to strong waves or tides (e.g. Ferrarin et al., 2008; Santos et al., 2009a). However, their precise location and sampling is not always an easy task, especially where artificial submarine emissary are present. Electromagnetic (Teatini et al., 2011) and thermal infrared methods (Mejías et al., 2012) were recently proposed to locate FSGD, but they suppose costly airborne surveys and might not be systematically adapted to locate artificial emissaries.

In this paper, a radon–radium mass balance was performed to quantify SGD to one of the largest Mediterranean coastal lagoon, the Mar Menor in Southeast Spain, connected to an intensively irrigated agricultural watershed. The most representative SGD composition, reflecting both FSGD and RSGD was selected after a detailed sampling of piezometers and sediments under the lagoon combined with hydrodynamic calculations. As the main river carries water from groundwater drainage (García-Pintado et al., 2007), a non-negligible source of radionuclides was expected. Hidden inputs of radionuclides originated by brines from groundwater desalination were also expected (Baudron et al., 2014), but with no information about their location and flux. In order to (i) understand the potential impact of surface water discharge to

the lagoon, (ii) localize additional undocumented inputs and (iii) decipher surface inputs from SGD, the radionuclides survey was combined with a numerical simulation of the lagoon hydrodynamics. Until now, such a combination was implemented only once, in the Venice lagoon (Ferrarin et al., 2008; Rapaglia et al., 2010), but with the differing objectives of comparing residence times and estimating the seasonal and temporal variability of SGD.

## 2. Site description

### 2.1. The Mar Menor coastal lagoon

Located in semiarid SE Spain, the Mar Menor (135 km<sup>2</sup>) is one of the largest coastal lagoons of the Mediterranean Sea (Fig. 1). It represents a volume of  $591 \cdot 10^6$  m<sup>3</sup> with a mean depth of 4.5 m and a maximum depth close to 6.5 m. Water temperature at the bottom of the lagoon ranges between 7.8 °C in winter and 30.2 °C in summer (López-Castejón and Gilabert, personal communication) in coherence with the atmospheric temperature variations. The Mar Menor is separated from the Mediterranean Sea on its eastern side by a 22 km long narrow sandy bar system (La Manga; width between 100 and 1200 m) tied to four volcanic outcrops. Other volcanic outcrops in the lagoon form three small islets. Three inlets connect the lagoon with the Mediterranean Sea (Fig. 1), although the main water exchange occurs through the central one, the Estacio channel that was widened and dredged in 1973 to make it navigable.

Due to the scarcity of precipitations (300 mm/y), which mainly occur during storm events, the limited surface runoff does not compensate the high evaporation of the lagoon, requiring a net inflow from the Mediterranean Sea of about  $130 \cdot 10^6$  m<sup>3</sup>/y (Cabezas, 2009). The lagoon is therefore hypersaline, around 47 psu. Calculated renewal time ranges from 0.66 to 1.2 year (Pérez-Ruzafa et al., 2005; Cabezas, 2009; Martínez-Alvarez et al., 2011). Water circulation can be very dynamic and is mainly controlled by wind and atmospheric pressure (Arévalo, 1988). Despite a weak stratification in the early morning, the water column can be considered homogeneous (López-Castejón and Gilabert, personal communication). Still, local stratification can be found in some areas located close to the inlets and affected by the Mediterranean Sea water. Maximum variation of the water level in the lagoon, recorded by two Acoustic Doppler Current Profilers (ADCP, see Section 3), is 70 cm. Tidal variations are limited to 2–3 cm, as tides are mostly choked in the inlets.

### 2.2. The Campo de Cartagena coastal aquifer system

The Mar Menor is bordered to its North, West and South sides by a detrital Quaternary aquifer (1200 km<sup>2</sup>), the upper layer of the Campo de Cartagena multi-aquifer system (Jiménez-Martínez et al., 2012; Baudron et al., 2013a), which supports intensive irrigated agriculture (Perni and Martínez-Paz, 2013). Some authors assumed a fault system under the Mar Menor (e.g. Lillo Carpio, 1978) or at its western limits (Rodríguez Estrella, 2004). However, the recent review of existing information by García-Aróstegui et al. (2012) did not identify such fault systems along the lagoon. We therefore assume that the Quaternary aquifer fully underlies the lagoon.

A main peculiarity of the area is the existence of an unknown number of small desalination plants used to lower the salinity of brackish groundwater (Lorenzen et al., 2012) before irrigating. The final destination of these brines is uncertain: they are partly injected in the aquifers, released to the surface watershed or directly to the Mar Menor lagoon. A rough estimation of the volume of brines gives  $10^7$  m<sup>3</sup>/y, considering an efficiency of 50% for reverse osmosis (as usually observed) and a contribution of



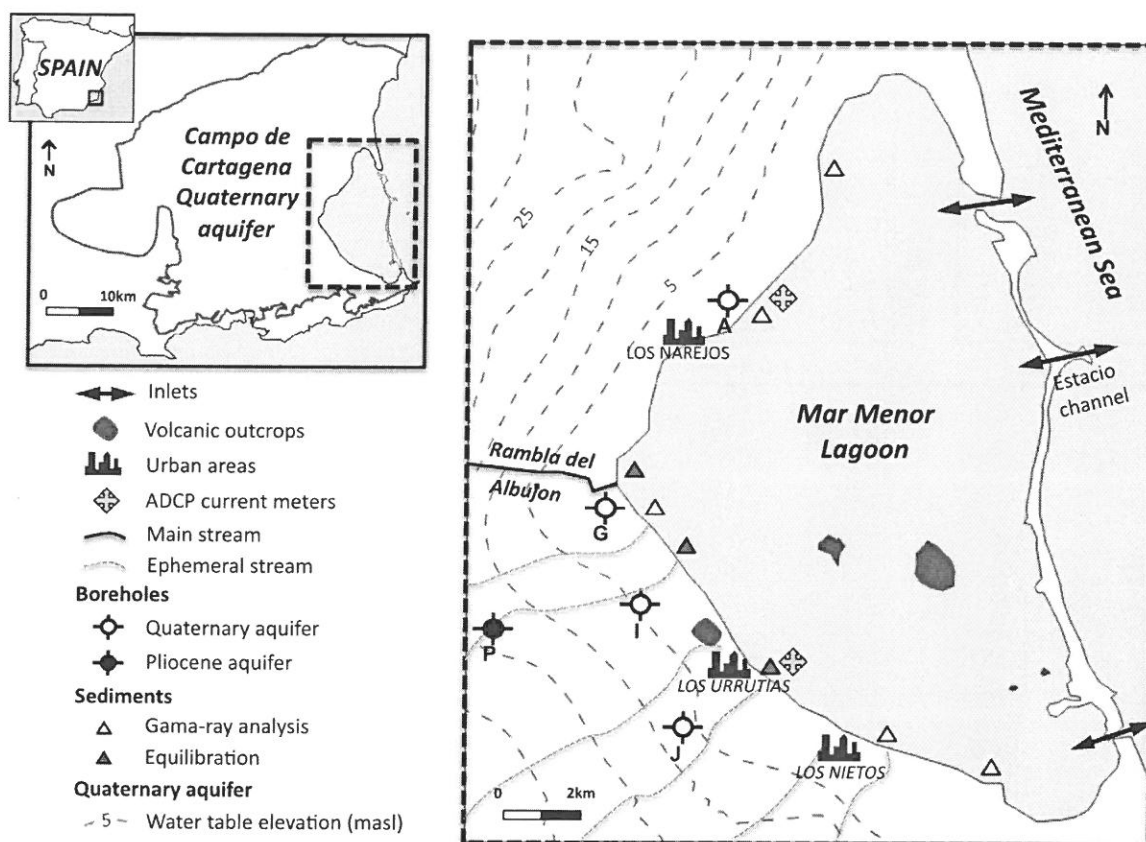


Fig. 1. Location of the study area, showing sampled boreholes, sediments, Quaternary aquifer water table elevation (based on IEA, 2011), location of the Acoustic Doppler Current Profilers (ADCP) and location of inlets.

groundwater desalination to irrigation of about 5% (based on field survey).

### 2.3. The Rambla del Albujón watershed

A network of ephemeral streams locally called “ramblas” drains the area, transferring rainwater sporadically during the rainfall events (Baudron et al., 2013b). Some of the southern ones are connected to the Cartagena-La Unión mining area. The main stream is the Rambla del Albujón (40 km long). Thereafter named “the Rambla”, it constitutes the axial drainage of the Campo de Cartagena and artificially concentrates water from neighboring watersheds that used to flow directly to the lagoon. Since the 1980s, a permanent flow has appeared in the last kilometers of the riverbed (Velasco et al., 2006). It now represents  $7.7 \cdot 10^6 \text{ m}^3/\text{y}$  (IEA, 2011) at the mouth (R1 in Fig. 2). This value is mainly supported by the natural drainage of the Quaternary aquifer, whose water table level has risen in response to increased irrigation return flow, together with numerous agricultural drains, artificial releases of unknown origin, most probably brines from private desalination plants, and sporadic discharge from a sewage water treatment plant. Up to day, the following three main artificial releases could be located: R2 and R3 (Fig. 2) discharge respectively  $0.8 \cdot 10^6 \text{ m}^3/\text{y}$  and  $2.4 \cdot 10^6 \text{ m}^3/\text{y}$  (IEA, 2011) to the stream, a few tenths of meters upstream the mouth, while R4 discharges  $2.9 \cdot 10^6 \text{ m}^3/\text{y}$  directly to the lagoon (IEA, 2011), a few tenths of meters northwards from R1. The state of anthropization of this watershed is a unique case that causes complications for SGD assessment, as high radionuclide activities are potentially carried by surface water to the lagoon.

## 3. Methods

### 3.1. Sampling

#### 3.1.1. Continental groundwater, brines and surface water

Groundwater samples were collected following two specific objectives. The first one was to define the composition of continental groundwater, representative for the regional flow in the Quaternary aquifer, and discuss it in comparison with the other potential SGD term (recirculated seawater). The second objective was to assess the contribution of Quaternary groundwater to the surface watershed by natural drainage to streams. To this end, groundwater sampling was conducted in 2010, 2011 and 2012 in four Quaternary boreholes (A, G, I, J) located on the coastal border of the Mar Menor (Fig. 1). Samples were extracted with an electric pump after stabilization of the physical and chemical parameters (pH, EC, temperature, eH). Before sampling, hydraulic heads at wells were measured. The data was then summed to a wider database by IEA (2011) in order to obtain the water table elevation curves displayed in Fig. 1.

As aforementioned, brines from desalinated groundwater can be released either to the aquifers, to the watershed, or directly to the lagoon. In order to assess how  $^{222}\text{Rn}$  was affected during the desalination process, water samples were taken from a reverse osmosis plant at three steps: input groundwater from the tubewell ( $D_{\text{in}}$ ), desalinated water ( $D_{\text{out1}}$ ) and brines ( $D_{\text{out2}}$ ). In this particular case,  $D_{\text{in}}$  corresponds to groundwater from the confined Pliocene aquifer (sandstone).

In order to characterize qualitatively and quantitatively the spatio-temporal variability of the composition of surface water

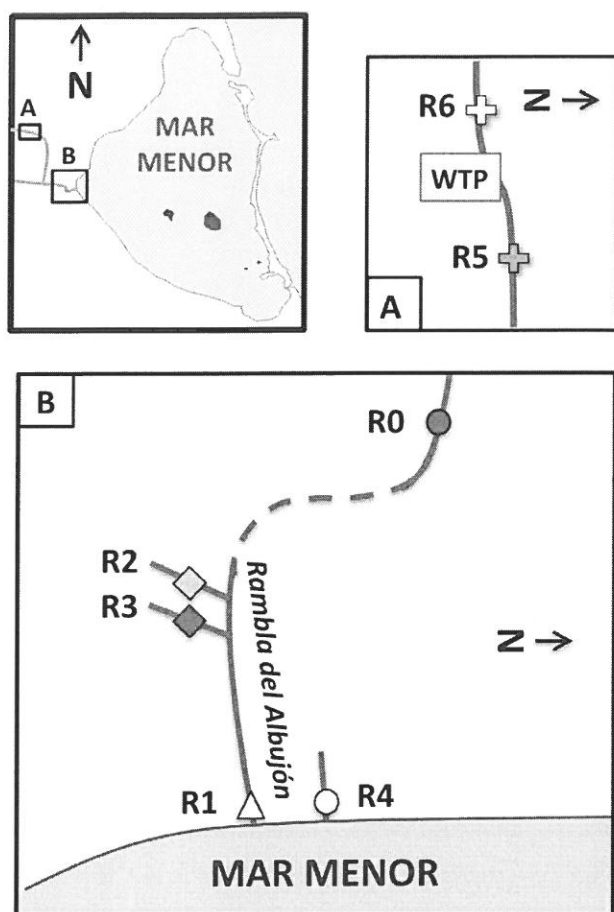


Fig. 2. Schematic of the Rambla del Albuñón watershed and location of the surface water sampling (not to scale). Discontinuous line indicates discontinuous presence of water. WTP is an urban water treatment plant. R1 is the outlet of Rambla del Albuñón to the Mar Menor lagoon; R2, R3 and R4 are tributaries of unknown origin and R0 represents the upper part of the surface watershed.

composition discharge to the lagoon, a series of key locations were sampled along the Rambla del Albuñón watershed, in the main course of the river and in artificial releases (Fig. 2). The main contributing discharge points (R0, R1, R2, R3, R4) were sampled several times during the 2011 and 2012 surveys (Table 2).

Physical and chemical parameters were measured with a Hach Lang multi parameter device. Samples were collected in 50 mL polypropylene bottles for anions. Samples for radon ( $^{222}\text{Rn}$ ) were collected in 250 mL glass bottles and samples for radium (Ra) isotopes in 15 L containers.

### 3.1.2. Lagoon and seawater

The seasonal variations of agricultural practices and the impact of climatic conditions (wind, temperature, salinity) on the distribution of  $^{222}\text{Rn}$  and Ra isotopes in the lagoon were characterized along three sampling campaigns in November 2010 (winter season), July 2011 (summer season) and January 2012 (winter season). The 2010 campaign mostly consisted in a  $^{222}\text{Rn}$  survey along the western coast of the Mar Menor (see Section 3.2.2), together with the collection of five discrete samples for radium isotopes. In 2011, a wider area was sampled for  $^{222}\text{Rn}$  including the central part of the lagoon, the surroundings of a volcanic island and the Mediterranean Sea, while ten discrete samples were collected for radium inside the lagoon and one in the Mediterranean Sea. In 2012, a wider perspective of the lagoon and the Mediterranean

Sea was obtained with new  $^{222}\text{Rn}$  surveys while fourteen discrete samples in the lagoon and one in the Mediterranean Sea were collected for radium. In addition, radon activity was also measured for time-series at a fixed location in an area sheltered from currents (the Los Urrutias harbour) on July, 10 and 11 2011. The two aforementioned ADCP current meters (Aquadopp, Nortek) were deployed at 4 m depth to measure temperature and water level together with current velocity and direction. This data was then used to validate the hydrodynamic model. The first ADCP was located at the NW lagoon coast, close to Los Narejos, the second close to Los Urrutias (Fig. 1).

Samples for  $^{222}\text{Rn}$  were directly processed on board, as detailed in Section 3.2.2. Samples for radium isotopes were collected in 15 L containers. Turbidity, pH, temperature, electric conductivity (EC), salinity and chlorophyll were continuously recorded by a YSI V6600 V2 multiparametric probe, together with the GPS location.

### 3.1.3. Sediments

Eight saturated sediments were collected from the sea bottom of the Mar Menor in July 2011 and January 2012 (Fig. 1) in order (i) to measure the radium and radon pore water activities in equilibrium with the sediment, (ii) to estimate the diffusive production of radionuclides from the sediments underlying the lagoon and (iii) to assess whether the release of radionuclides from resuspended sediments could be a significant additional source of radionuclides to the lagoon.

## 3.2. Analytical techniques

### 3.2.1. Radium isotopes

Radium isotopes were extracted by passing sample waters by gravity through a PVC cartridge filled with 20 g dry weight of manganese oxide-impregnated acrylic fiber ("Mn-fiber"). The water flow rate was checked to be less than 1 L per minute, in order to insure the retention capacity of the Mn-fiber to be higher than 97% (Moore, 2008). Before processing the sample, the water content of each Mn-fiber was kept between 0.4 and 1.1  $\text{g}_{\text{H}_2\text{O}}/\text{g}_{\text{fiber}}$  in order to get maximum emanation efficiency (Sun and Torgersen, 1998). The samples were processed with either with RaDeCC system for  $^{223}\text{Ra}$  and  $^{224}\text{Ra}$  in January 2012 (Radium Delayed Coincidence Counting) or with RAD-7 system (radon-in-air detector, Durridge, Co.) for  $^{224}\text{Ra}$  in November 2010 and July 2011.

$^{223}\text{Ra}$  and  $^{224}\text{Ra}$  activity measurements with RaDeCC were calibrated using 4 in-house mono-isotope standards of  $^{227}\text{Ac}$  and  $^{232}\text{Th}$  (parents of  $^{223}\text{Ra}$  and  $^{224}\text{Ra}$  respectively) and 4 multi-isotope standards, containing  $^{227}\text{Ac}$ ,  $^{232}\text{Th}$  and  $^{226}\text{Ra}$ . All standards were prepared according to the technique of Scholten et al. (2010). Detection efficiencies of our four detectors were very similar and close to the values reported in Scholten et al. (2010). Changes of efficiencies with time are within the error range and thus not significant. All errors were calculated according to Garcia-Solsona et al. (2008).

$^{228}\text{Th}$  activity in water was processed with RaDeCC one month after collection measuring supported  $^{224}\text{Ra}$ , in equilibrium with  $^{228}\text{Th}$ .  $^{227}\text{Ac}$  activity in water was processed with RaDeCC 3 months after collection measuring supported  $^{223}\text{Ra}$  in equilibrium with  $^{227}\text{Ac}$ .

$^{224}\text{Ra}$  activities were determined using RAD7 system by placing the Mn-fiber in a glass cartridge hermetically closed during 10 min in order to reach the equilibrium between  $^{224}\text{Ra}$  and  $^{220}\text{Rn}$  (thoron). The cartridge is connected to RAD-7 system and the protocol is chosen to analyze thoron. The RAD-7 detection efficiency for  $^{224}\text{Ra}$  was calculated using two of the standards described above: one standard of  $^{232}\text{Th}$  and one multi-isotope standard (containing  $^{232}\text{Th}$  and  $^{226}\text{Ra}$ ). The detection efficiency calculated using both standards was similar. Cross comparisons of  $^{224}\text{Ra}$  activities

measured with the RAD7 and RaDeCC detectors on one standard and three sample fibers (in the range of 10–100 Bq/m<sup>3</sup>) returned similar results within uncertainties.

<sup>226</sup>Ra activities in the lagoon were determined in four samples through radon emanation. Mn-fibers were placed in glass cartridge hermetically closed during 3 weeks in order to reach equilibrium between <sup>226</sup>Ra and <sup>222</sup>Rn and then connected to a RAD-7 system. The RAD-7 efficiency for <sup>226</sup>Ra was determined using the multi-isotope standard.

### 3.2.2. Radon isotopes

The <sup>222</sup>Rn activities of lagoon water and seawater were measured according to Dulaiova et al. (2005) by means of two radon-in-air detectors routed simultaneously through one single air–water exchanger (RAD-Aqua, DurrIDGE). Water was pumped on subsurface at a constant flow rate of 2.5 L/min and filtered through an 80 mm cartridge. The boat was always moving and data was integrated each 15 min (corresponding to one run). Since the RAD-7 determines <sup>222</sup>Rn activity by measuring the decay of the daughter <sup>218</sup>Po considered to be in equilibrium with <sup>222</sup>Rn after 15 min (5 half-lives of <sup>218</sup>Po; Stieglitz, 2005), the radon activity of each run was associated with the geographical position of the boat 15 min before. The longer equilibration time from high to low activity (Stieglitz et al., 2010) was not taken into account. Analytical uncertainties (reported in Fig. 4) are based on counting statistics, and are typically around 45% (2σ) for our configuration (two RAD-7 and 15 min run) and water activities. For groundwater samples, <sup>222</sup>Rn activities were analyzed using a RAD-H<sub>2</sub>O extension of the RAD-7 using 250 mL samples. All <sup>222</sup>Rn activities were corrected from temperature and humidity effect (using the DurrIDGE Capture software) as well as from salinity effect (according to Schubert et al., 2012). Analytical uncertainties are based on counting statistics.

### 3.2.3. Radon and radium in sediments and porewater

Five sediment samples (Fig. 1) were analyzed by gamma ray spectrometry at CEREGE in order to assess their <sup>226</sup>Ra and <sup>228</sup>Ra activities (using the 295 and 911 keV of <sup>214</sup>Pb and <sup>228</sup>Ac respectively). The mean Mar Menor sediment porosity was estimated by comparing the wet and dry weight (Corbett et al., 1998) of 4 sediment samples.

The method commonly used to estimate <sup>222</sup>Rn content in porewater is based on equilibration experiments (Corbett et al., 1998; Kluge et al., 2012; Burnett et al., 2007). According to the protocol described in Corbett et al. (1998), five experiments were done with 500 g of dry sediment put in closed glass bottles with 900 mL of Ra-free seawater, previously passed through Mn-fiber to remove all radium isotopes. The system was left for more than one month to allow the equilibrium between water over and within the sediment. The overlying water was collected and analyzed with RAD-7+Rad-H<sub>2</sub>O system. The equilibration experiments and analysis were performed at the room temperature (appreciatively 20 °C).

We used the same protocol to estimate <sup>223</sup>Ra and <sup>224</sup>Ra content in porewater, assuming that 5 months after the bottle closing (more than 10 times the <sup>224</sup>Ra and <sup>223</sup>Ra half-lives) the overlying water is in equilibrium with porewater. This hypothesis is based on Beck et al. (2007, 2008), who added regularly Ra-free seawater to a core and analyzed the overlying waters for various time intervals. They observed a clear enrichment of overlying water associated with diffusion tending towards equilibrium after more than 100 h. For <sup>223</sup>Ra and <sup>224</sup>Ra, the overlying water of 3 equilibration experiments was analyzed with RaDeCC system.

For both radon and radium, we applied a correction factor that takes into account the difference of water/sediment ratio between our experiment and the lagoon sediment (the mean measured porosity equals 0.5). The activity in porewater in equilibrium with

the sediment ( $C_{eq}$ ) is thus estimated as follows (modified after Stieglitz et al., 2013):

$$C_{eq} = C_{incubation} * R_{Lab} / R_{field}$$

where  $C_{incubation}$  the activity measured within the bottle,  $R_{Lab}$  and  $R_{field}$  are the water/sediment volume ratios respectively in the bottle and in the field.

### 3.2.4. Other tracers

Nitrate in groundwater and surface water was analyzed by chromatography (University of Cartagena). Nitrate in the lagoon and seawater was continuously recorded by a SUNA V2 UV (Satlantic) equipment, together with the GPS location. It had been previously calibrated with a standard solution of NaNO<sub>3</sub> prepared in the laboratory at the range of expected nitrate concentrations in the lagoon water.

### 3.3. Hydrodynamic modeling of the lagoon

Prior to each simulation, the model ran for 6 days with all the hydrodynamic forcings in order to let it spin up before the river input was inserted into the model. Then, the hydrodynamic dispersion of the input of <sup>222</sup>Rn and <sup>224</sup>Ra generated by the Rambla into the lagoon (thereafter called "plume") was modeled and compared to the measurements. It was used as a diagnostic tool to locate point sources of radionuclides inside the lagoon in areas not attained by the plume during the days of modeling: if such activities could not be explained by the plume, additional sources of radionuclides would be evidenced. The introduction of the tracer in the model started 6 days before the days of sampling, i.e. approximately 1.5 half-life of decay for <sup>222</sup>Rn. This decay provided an additional criterion for evidencing the non-Rambla origin of measured values, as no more than 25% of the input level of <sup>224</sup>Ra and <sup>222</sup>Rn was expected to persist at the time of sampling in the oldest parts of the plume.

The model considered mean values for discharge, <sup>222</sup>Rn, <sup>224</sup>Ra and <sup>223</sup>Ra activities of the Rambla, as well as for lagoon activities and Mediterranean Sea activities. The data was provided by the field surveys, using the same mean values as in the mass balance (see Sections 4.1.2 and 4.1.3).

The hydrodynamic simulations of the lagoon were performed using ROMS-AGRIF (Debreu et al., 2012), the ROMS version developed by the Institut de Recherche pour le Développement (IRD) using the AGRIF grid refinement procedure developed at the LJK-IMAG (Laboratoire Jean Kuntzmann, Grenoble, France). The Mediterranean Sea grid (150 m resolution) was nested to the Mar Menor grid (40 m) and to the inlets grids (of 5–20 m). All nesting grids were bidirectional. The Mediterranean Sea model was forced with sea level fluctuations recorded by a sea level gauge in the Mediterranean Sea (northern part of the study area). The lagoon model was forced with hourly winds recorded at the meteorological station on the northwest coast of the lagoon in the San Javier Airport (run by the Spanish Meteorological Agency – AEMET). As aforementioned, modeling results were validated against two ADCP current meters (Fig. 1). The validation parameters for a 15 days period simulation were: Root Mean Square error (RMS) and correlation coefficient.

## 4. Results

### 4.1. Geochemistry

#### 4.1.1. Continental groundwater

Average temperature of 20.9 ± 0.9 °C was similar to the mean annual temperature of surface water (Fig. 3). Electrical

conductivity (EC) ranged between 5.3 and 12.6 mS/cm and displayed minor change with time.  $^{222}\text{Rn}$  activities in Quaternary groundwater were heterogeneous, between  $2100 \pm 800$  and  $26,500 \pm 1500 \text{ Bq/m}^3$ , with a mean value around  $14,000 \text{ Bq/m}^3$  and without any correlation with EC (Fig. 3).  $^{224}\text{Ra}$  activities in the Quaternary aquifer varied between  $9.8 \pm 0.9$  and  $75.3 \pm 2.2 \text{ Bq/m}^3$  (Table 1 and Fig. 3), with no significant  $^{224}\text{Ra}$  changes in time. The average  $^{224}\text{Ra}$  was  $55 \pm 13 \text{ Bq/m}^3$ , dismissing borehole A characterized by lower radium activities as for  $^{222}\text{Rn}$ .  $^{223}\text{Ra}$  only measured in two boreholes varied by a factor of four ( $0.5 \pm 0.3$ – $1.8 \pm 0.8 \text{ Bq/m}^3$ ). Deep groundwater ( $D_{\text{in}}$  from the Pliocene aquifer) displayed much higher radon activity (about  $75,000 \pm 3400 \text{ Bq/m}^3$ ,

EC = 5.7C mS/cm) than the maximum value of Quaternary samples ( $26,500 \pm 2000 \text{ Bq/m}^3$ ). The product of desalination by reverse osmosis of Pliocene groundwater ( $D_{\text{out1}}$ ) had  $^{222}\text{Rn}$  activities of approximately  $59,000 \pm 6000 \text{ Bq/m}^3$  (EC = 0.5C mS/cm) while the released brine ( $D_{\text{out2}}$ ) reached approximately  $69,000 \pm 5000 \text{ Bq/m}^3$  (EC = 16.8 mS/cm).

#### 4.1.2. Surface waters

Combining our physico-chemical results with the ones from IEA (2011), all tributaries (except R3) and main streams R1 and R4 showed a similar seasonal variability (winter/summer) for temperature: around  $15^\circ\text{C}$  in winter and between  $24$  and  $28^\circ\text{C}$  in summer (Fig. 3). R3 appeared more specific since it displayed less variation in temperature (stable around  $18^\circ\text{C}$ , with a high value at  $25^\circ\text{C}$ ) and higher EC values (between 20 and 25 mS/cm). R1 was characterized by a large range of variation of EC ( $12.2$ – $16.5 \text{ mS/cm}$ ) not correlated with the seasonality. In addition, we observed an increase of EC with the water discharge simultaneously for R1 and R3.

Regarding  $^{222}\text{Rn}$ , similar and almost constant activities were found in R1 and R4 with average values of  $1900 \pm 400$  and  $2000 \pm 800 \text{ Bq/m}^3$  in July 2011 and  $2900 \pm 500$  and  $2600 \pm 200 \text{ Bq/m}^3$  in January 2012 (detailed data in Table 2). All these values were notably higher than those commonly found in literature for rivers (e.g.  $4$ – $11 \text{ Bq/m}^3$  in Gattacceca et al., 2011;  $80$ – $500 \text{ Bq/m}^3$  in Lefebvre et al., 2013). Indeed, activities were even higher in R2 and especially R3 pipe that ranged from  $10,000 \pm 3000$  to  $18,000 \pm 3000 \text{ Bq/m}^3$  (Table 2). Upstream (R6) and downstream (R5) the release from the water treatment plant, we measured radon activities of  $2200 \pm 800$  and  $900 \pm 400 \text{ Bq/m}^3$ , respectively.

Regarding radium, activities were especially high in R1, higher than for groundwater.  $^{224}\text{Ra}$  varied by a factor of two between July 2011 and January 2012 but remained constant in January 2012 within a 3-day interval ( $108 \pm 11$  and  $5.0 \pm 1 \text{ Bq/m}^3$  for  $^{224}\text{Ra}$  and  $^{223}\text{Ra}$  respectively). R3 was characterized by twice more  $^{224}\text{Ra}$  but similar  $^{223}\text{Ra}$  activities than R1. As for radon, such high radium activities are very uncommon in surface waters (e.g. Beck et al., 2007).

For hydrodynamic modeling and mass balance purposes, the mean  $^{222}\text{Rn}$  activities in R1 and R4 are  $2000 \pm 300 \text{ Bq/m}^3$  for July 2011 and  $2900 \pm 300 \text{ Bq/m}^3$  for January 2012.

Accordingly, mean activities are taken to be  $64 \pm 13$  (2011) and  $108 \pm 7 \text{ Bq/m}^3$  (2012) for  $^{224}\text{Ra}$  and  $5.1 \pm 0.3 \text{ Bq/m}^3$  (2012) for

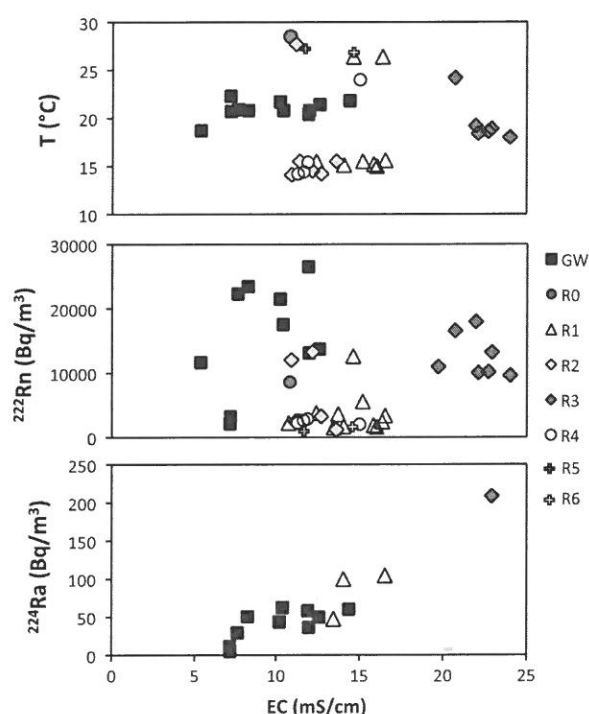


Fig. 3. Temperature,  $^{222}\text{Rn}$  and  $^{224}\text{Ra}$  vs EC in Quaternary groundwater, main streams (R1, R4) and tributaries (R0, R2, R3).

Table 1

Physico-chemical parameters and radionuclide data measured in groundwater. Coordinates are given in the Universal Transverse Mercator (UTM) geographic coordinate system. Errors on  $^{224}\text{Ra}$ ,  $^{223}\text{Ra}$  and  $^{222}\text{Rn}$  values are  $2\sigma$ .

Sample ID	Water type	X (UTM)	Y (UTM)	Bore-hole depth (m)	Sampling date	EC (mS/cm)	pH	Temp ( $^\circ\text{C}$ )	$^{224}\text{Ra}$ ( $\text{Bq/m}^3$ )	$^{223}\text{Ra}$ ( $\text{Bq/m}^3$ )	$^{222}\text{Rn}$ ( $\text{Bq/m}^3$ )	$\text{NO}_3^-$ (mg/l)
I	Quaternary	688,594	4,173,998	12	23-November-10	10.4	7.1	20.8	$75.3^{\text{a}} \pm 2.2$	–	$17,500 \pm 1900$	223.8
				12	07-July-11	10.2	7.1	21.7	$52.8^{\text{a}} \pm 8.5$	–	$21,500 \pm 2500$	249.1
A1	Quaternary	691,755	4,181,757	25	20-November-10	7.2	7.4	20.7	$10.8^{\text{a}} \pm 0.7$	–	$3200 \pm 700$	167.5
				25	07-July-11	7.2	7.5	22.3	$16.3^{\text{a}} \pm 4.6$	–	$2100 \pm 800$	225.6
				25	21-January-12	5.3	7.6	18.7	–	–	$11,600 \pm 2000$	144.4
A2		691,755	4,181,757	7	21-November-10	7.2	7.6	20.7	$9.8^{\text{a}} \pm 0.9$	–	$2200 \pm 700$	174.7
G	Quaternary	687,746	4,176,927	12	24-November-10	12.6	6.9	21.4	$60.3^{\text{a}} \pm 2.6$	–	$13,700 \pm 1800$	38.3
				12	07-July-11	12.0	6.9	20.8	$60.8^{\text{a}} \pm 13.2$	–	$13,100 \pm 1900$	29.0
				12	21-January-12	11.9	6.9	20.4	$49.0 \pm 5.0$	$1.80 \pm 0.80$	$26,500 \pm 1500$	36.0
J	Quaternary	689,920	4,170,500	12	07-July-11	7.6	7.1	20.9	$34.8^{\text{a}} \pm 10.2$	–	$22,300 \pm 2500$	389.0
				12	21-January-12	8.2	7.1	20.8	$50.0 \pm 6.0$	$0.50 \pm 0.30$	$23,400 \pm 5900$	351.6
$D_{\text{in}}$	Pliocene	683,698	4,173,652	150	13-February-12	5.7	7.3	–	–	–	$74,900 \pm 3400$	–
$D_{\text{out1}}$	<sup>b</sup>				13-February-12	0.5	6.5	–	–	–	$58,900 \pm 5600$	–
$D_{\text{out2}}$	<sup>c</sup>				13-February-12	16.8	7.5	–	–	–	$68,700 \pm 4800$	–

<sup>a</sup>  $^{224}\text{Ra}$  values measured with RAD7 system.

<sup>b</sup> Desalinated water from  $D_{\text{in}}$ .

<sup>c</sup> Brines from  $D_{\text{in}}$ .



**Table 2**

Physical–chemical parameters and radionuclide data measured in rivers. Coordinates are given in the Universal Transverse Mercator (UTM). Errors on  $^{224}\text{Ra}$ ,  $^{223}\text{Ra}$  and  $^{222}\text{Rn}$  values are  $2\sigma$ .

Sample ID	Sampling date	EC (mS/cm)	pH	Temp (°C)	$^{224}\text{Ra}$ (Bq/m <sup>3</sup> )	$^{223}\text{Ra}$ (Bq/m <sup>3</sup> )	$^{222}\text{Rn}$ (Bq/m <sup>3</sup> )	$\text{NO}_3^-$ (mg/l)	Discharge (10 <sup>6</sup> m <sup>3</sup> /y)
R0	10-July-11	10.8	–	28.5	–	–	8600 ± 2700	–	–
R1 (main outlet)	12-July-11	13.5	–	–	63.6 <sup>a</sup> ± 13.0	–	1500 ± 700	–	–
	13-July-11	16.4	–	26.4	–	–	2400 ± 2400	–	–
	17-January-12	13.7	–	–	–	–	3600 ± 1900	–	–
	18-January-12	10.7	–	–	–	–	2200 ± 1000	–	–
	19-January-12	12.4	–	15.5	–	–	3800 ± 1100	–	–
	20-January-12	14.0	8.0	15.1	121.0 <sup>a</sup> ± 8.1	–	1600 ± 1300	159.6	8.7
	Duplicate	–	–	–	99.0 ± 16.0	5.6 ± 1.1	–	–	–
	21-January-12	15.2	7.7	15.5	–	–	5500 ± 3600	218.9	9.4
	22-January-12	16.5	7.9	15.6	104.0 ± 16.0	4.7 ± 1.1	3400 ± 900	114.0	–
	24-January-12	15.8	7.9	15.2	–	–	1800 ± 700	–	7.2
	25-January-12	16.0	–	15.0	–	–	1600 ± 1300	–	–
	1-February-12	–	–	–	–	–	–	–	–
R2	10-July-11	11.1	–	27.7	–	–	2400 ± 400	–	–
	12-July-11	11.2	–	–	–	–	2500 ± 1500	–	–
	20-January-12	11.4	7.9	15.5	–	–	2500 ± 1400	138.8	0.4
	21-January-12	10.9	7.5	14.1	–	–	12,000 ± 1700	167.5	0.6
	22-January-12	12.2	7.6	14.5	–	–	13,200 ± 11,000	–	0.5
	24-January-12	13.6	8.1	15.5	–	–	1100 ± 1000	239.0	–
	25-January-12	12.7	–	14.2	–	–	3200 ± 1900	–	0.4
R3	10-July-11	20.7	–	24.2	–	–	16,600 ± 2500	–	–
	12-July-11	19.7	–	–	–	–	11,000 ± 3100	–	–
	20-January-12	22.1	7.3	18.4	–	–	10,000 ± 2500	230.8	1.7
	21-January-12	21.9	7.2	19.2	–	–	17,900 ± 2700	237.1	2.0
	22-January-12	22.9	7.4	18.9	208.0 ± 24.0	5.6 ± 2.0	13,200 ± 4200	–	3.0
	24-January-12	22.7	7.5	18.6	–	–	10,100 ± 3200	251.9	–
	25-January-12	24.0	–	18.0	–	–	9600 ± 3600	–	2.1
R4 (outlet)	12-July-11	15.0	–	24.0	–	–	2000 ± 800	–	–
	22-January-12	11.3	8.1	14.2	–	–	2200 ± 500	152.0	2.5
	24-January-12	11.9	7.6	15.4	–	–	2800 ± 400	223.0	–
	25-January-12	11.6	–	14.4	–	–	2600 ± 900	232.4	–
R5	12-July-11	11.4	–	27.4	–	–	900 ± 400	–	–
R6	12-July-11	14.5	–	26.8	–	–	2200 ± 800	–	–

<sup>a</sup>  $^{224}\text{Ra}$  values measured with RAD7 system.

$^{223}\text{Ra}$ . In order to calculate mean annual river fluxes to the Mar Menor (Table 4), these values are combined to a mean discharge of  $1.04 \cdot 10^7 \text{ m}^3/\text{y}$  (R1 + R4) for both sampling campaigns.

#### 4.1.3. Lagoon and Sea waters

Activities measured continuously during the three surveys in the Mar Menor ranged between 2.5 and 12.9, and 10 and 50 Bq/m<sup>3</sup> for  $^{224}\text{Ra}$  and  $^{222}\text{Rn}$ , respectively (Table 3, Figs. 4 and 5). In the Mediterranean Sea, activities were lower than 3 Bq/m<sup>3</sup> for  $^{222}\text{Rn}$  (Table 3) and values for  $^{224}\text{Ra}$  and  $^{223}\text{Ra}$  were similar to those reported for the open Mediterranean Sea by Garcia-Solsona et al. (2010) (around 0.3 and 0.1 for  $^{224}\text{Ra}$  and  $^{223}\text{Ra}$ ).  $^{224}\text{Ra}$  and  $^{222}\text{Rn}$  were clearly enriched along the western border of the Mar Menor in a wide area from los Narejos in the North to Los Nietos in the South (see location in Fig. 1). Maximum values for both radium and radon isotopes were always found in front of the Rambla mouth.

$^{222}\text{Rn}$  and nitrate data of November 2010 show a well-defined (15 km long) and symmetrical peak, slightly shifted to the South with respect to the Rambla (Fig. 4, left). A tiny but significant peak in turbidity was also recorded. Nitrate ranged from 0.04 to 0.5 mg/L.  $^{224}\text{Ra}$  activities were quite low too, but unfortunately no sample was taken at the location of the radon peak. High  $^{222}\text{Rn}$  spots were observed further north and south from the Rambla mouth. This observation was repeated in 2011 and 2012, as indicated by points 1–5 in Fig. 5.

In 2011, continuous measurements of  $^{222}\text{Rn}$ , nitrate and turbidity were performed on July 8 and 10 (Fig. 4, centre). Two peaks in turbidity were observed each day: one large peak in front of the Rambla mouth and another one 6 km to the south. The peak was

higher on July 8. Nitrate ranged between 0.18 and 10.3 mg/L, which is 25% more than in November. A nitrate peak was also observed each day: narrow and strictly in front of the Rambla mouth on July 8, it was wider and southwards on July 10. The maximum values of  $^{222}\text{Rn}$  were measured in front of the Rambla but showing a significant tailing southwards (as for turbidity) on July 8. On July 10, the radon peak shape was symmetrical and located in front of the Rambla.  $^{224}\text{Ra}$  activities showed the same peak shape.

On January 23 and 24, 2012, the wind speed was very low (<1 m/s) and turbidity near zero. The lowest nitrate values ranged between 0.11 and 0.5 mg/L, with a narrow and well-defined symmetrical peak strictly in front of the Rambla (Fig. 4, right). A similar feature was found both for  $^{222}\text{Rn}$  and  $^{224}\text{Ra}$ .

Results were interpolated by kriging with 100 m by 100 m cells (Fig. 5). Since the samples collected in November 2010 were all located on the western part of the Mar Menor, interpolation has a limited reliability for the central area at that time. Average activities for the lagoon were obtained by weighting the extrapolated value of each cell (Table 3) by the corresponding bathymetry. These values are used for the radiotracers mass balance calculation.

The  $^{222}\text{Rn}$  sampling at the Los Urrutias harbour between July 10 and 11, 2011 showed a smooth repetitive oscillation (Fig. 6), with a periodicity close to 12 h and values ranging from 23 to 35 Bq/m<sup>3</sup>.

$^{228}\text{Th}$ ,  $^{227}\text{Ac}$  and  $^{226}\text{Ra}$  activities were used to calculate the production of their radioactive daughters  $^{224}\text{Ra}$ ,  $^{223}\text{Ra}$ ,  $^{222}\text{Rn}$ , respectively. In the lagoon, the activities of  $^{228}\text{Th}$  range from 0.40 to 0.85 Bq/m<sup>3</sup> with a mean value of  $0.54 \pm 0.1 \text{ Bq/m}^3$ ,  $^{227}\text{Ac}$  is negligible and the activities of  $^{226}\text{Ra}$  range from 1.7 to 2.5 Bq/m<sup>3</sup> with a mean activity of  $2.1 \pm 0.3 \text{ Bq/m}^3$ .



**Table 3**

Physical-chemical parameters and radionuclide data measured in Mar Menor (MM-) and Mediterranean Sea waters (Med-). Coordinates are given in the Universal Transverse Mercator (UTM) geographic coordinate system. Errors on  $^{224}\text{Ra}$ ,  $^{223}\text{Ra}$  and  $^{222}\text{Rn}$  values are  $2\sigma$ .

Sample ID	Sample type	Sampling date	Depth (m)	EC (mS/cm)	Temp (°C)	$^{224}\text{Ra}$ (Bq/m <sup>3</sup> )	$^{223}\text{Ra}$ (Bq/m <sup>3</sup> )	$^{222}\text{Rn}$ (Bq/m <sup>3</sup> )	$\text{NO}_3^-$ (mg/l)
LO PAGAN	Mar Menor	23-November-10	2	–	–	–	–	$19.0 \pm 5.0$	–
MM1	Mar Menor	24-November-10	2	68.6	14.4	$4.0^a \pm 1.1$	–	$15.0 \pm 6.0$	0.26
MM2	Mar Menor	24-November-10	2	68.4	14.4	$3.6^a \pm 0.6$	–	$23.0 \pm 8.0$	0.27
MM3	Mar Menor	25-November-10	2	67.8	14.1	$2.8^a \pm 0.5$	–	$14.0 \pm 5.0$	0.28
MM4	Mar Menor	25-November-10	2	68.6	14.2	$4.6^a \pm 0.6$	–	$35.0 \pm 7.0$	–
Spatial integration		November 2010				3.8	–	19.4	0.34
MM10	Mar Menor	6-July-11	6	65.6	28.4	$5.6^a \pm 1.0$	–	–	–
MM11	Mar Menor	6-July-11	4	65.7	28.4	$7.5^a \pm 1.4$	–	–	–
MM12	Mar Menor	6-July-11	2	65.7	28.7	$10.2^a \pm 1.5$	–	–	–
MM13	Mar Menor	6-July-11	2	64.6	28.9	$6.2^a \pm 1.1$	–	–	–
MM14	Mar Menor	6-July-11	6	64.3	28.9	$6.8^a \pm 1.6$	–	–	–
MM15	Mar Menor	6-July-11	2	63.7	29.4	$12.4^a \pm 1.3$	–	–	–
MM16	Mediterranean Sea	9-July-11	8	56.8	25.7	$1.2^a \pm 0.6$	–	$3.0 \pm 3.0$	–
MM17	Mar Menor	9-July-11	6	63.5	28.9	$9.2^a \pm 2.0$	–	$11.0 \pm 6.0$	–
Spatial integration	Mar Menor	July 2011				7.6	–	12.6	0.30
MM18	Mar Menor	23-January-12	3	67.1	12.3	$3.20 \pm 0.30$	$0.13 \pm 0.04$	–	0.05
MM19	Mar Menor	23-January-12	3	66.9	12.3	$3.30 \pm 0.50$	$0.18 \pm 0.08$	$17.0 \pm 9.0$	0.16
MM20	Mar Menor	23-January-12	2	66.7	12.3	$12.9^a \pm 1.7$	–	$50.0 \pm 17.0$	0.50
MM20 duplicate	Mar Menor					$12.1 \pm 1.4$	$0.70 \pm 0.17$	–	–
MM21	Mar Menor	23-January-12	2	67.2	12.1	$4.8 \pm 0.4$	$0.29 \pm 0.09$	$31.0 \pm 13.0$	0.17
MM22	Mar Menor	23-January-12	2	67.2	12.5	$3.1 \pm 0.4$	$0.31 \pm 0.15$	$13.0 \pm 8.0$	0.17
MM23	Mar Menor	23-January-12	2	67.2	12.8	$2.9 \pm 0.4$	$0.23 \pm 0.08$	$23.0 \pm 11.0$	0.17
MM24	Mar Menor	23-January-12	3	66.9	13.1	$3.1 \pm 0.5$	$0.29 \pm 0.13$	$19.0 \pm 10.0$	0.16
MM25	Mar Menor	23-January-12	5	67.0	12.7	$2.5 \pm 0.3$	$0.19 \pm 0.08$	$12.0 \pm 8.0$	0.20
MM26	Mar Menor	23-January-12	5	67.1	12.6	$3.3 \pm 0.2$	$0.23 \pm 0.12$	$13.0 \pm 8.0$	0.23
MM27	Mar Menor	23-January-12	4	67.1	12.7	$3.0 \pm 0.3$	$0.14 \pm 0.04$	$22.0 \pm 11.0$	0.26
MM28	Mar Menor	24-January-12	6	67.0	12.5	$2.6 \pm 0.4$	$0.14 \pm 0.06$	$15.0 \pm 9.0$	0.12
MM29	Mar Menor	24-January-12	6	66.6	12.4	$1.6 \pm 0.2$	$0.09 \pm 0.03$	$11.0 \pm 7.0$	0.08
MM30	Mediterranean Sea	24-January-12	6	58.8	15.2	$0.34 \pm 0.06$	$0.04 \pm 0.03$	$3.0 \pm 2.0$	0.04
MM31	Mar Menor	24-January-12	3	66.8	13.5	$2.8 \pm 0.3$	$0.24 \pm 0.11$	$16.0 \pm 9.0$	0.12
Spatial integration	Mar Menor	January 2012				2.5	0.2	13.1	0.15

<sup>a</sup>  $^{224}\text{Ra}$  values measured with RAD7 system.

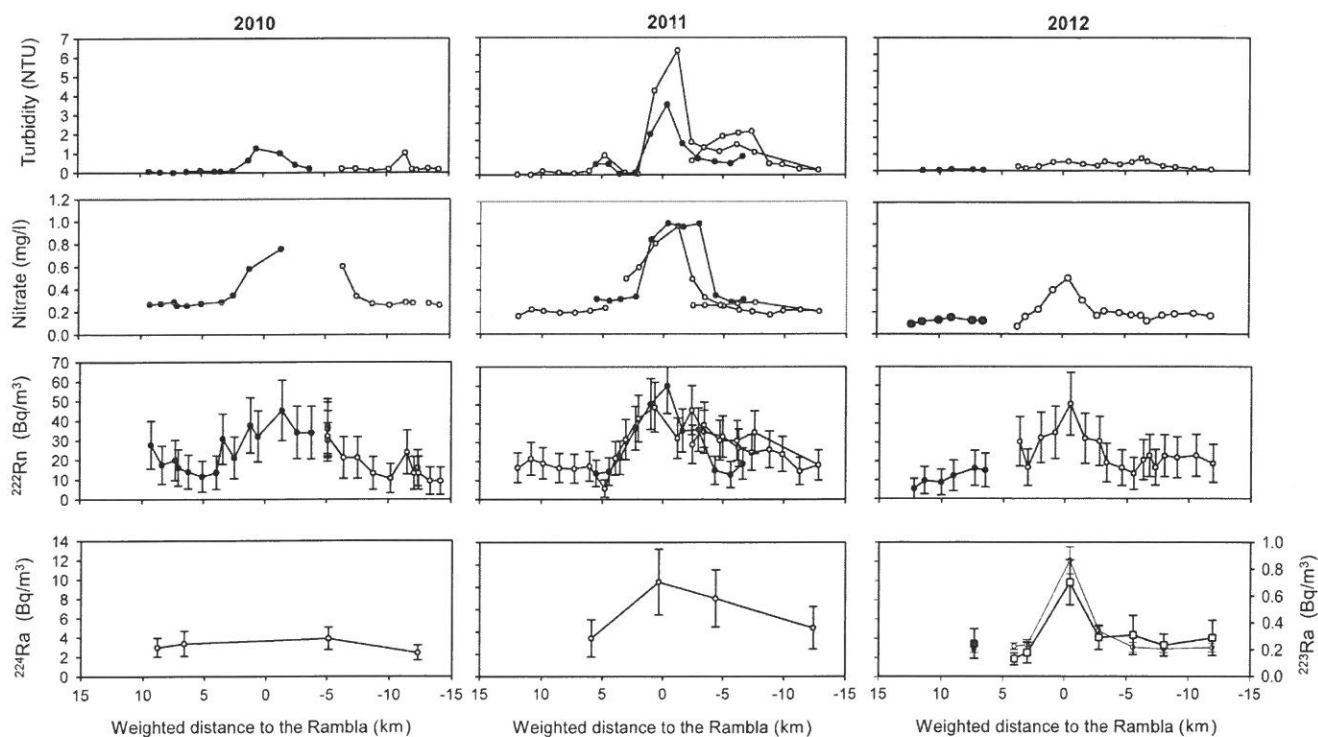


**Fig. 4.** Turbidity, nitrate content,  $^{222}\text{Rn}$ ,  $^{224}\text{Ra}$  and  $^{223}\text{Ra}$  activities along the western coastline of Mar Menor following a 2 m bathymetry. Negative distance refers to locations southwards from the Rambla del Albujón mouth. In 2010 (left), black and white circles stem for 24 and 25 November, respectively. In 2011 (centre), black and white circles stem for 10 and 8 July, respectively, except for  $^{224}\text{Ra}$  where white circles stem for 6 July. In 2012 (right), black and white circles and squares ( $^{223}\text{Ra}$ ) stem for 23 and 24 January, respectively.

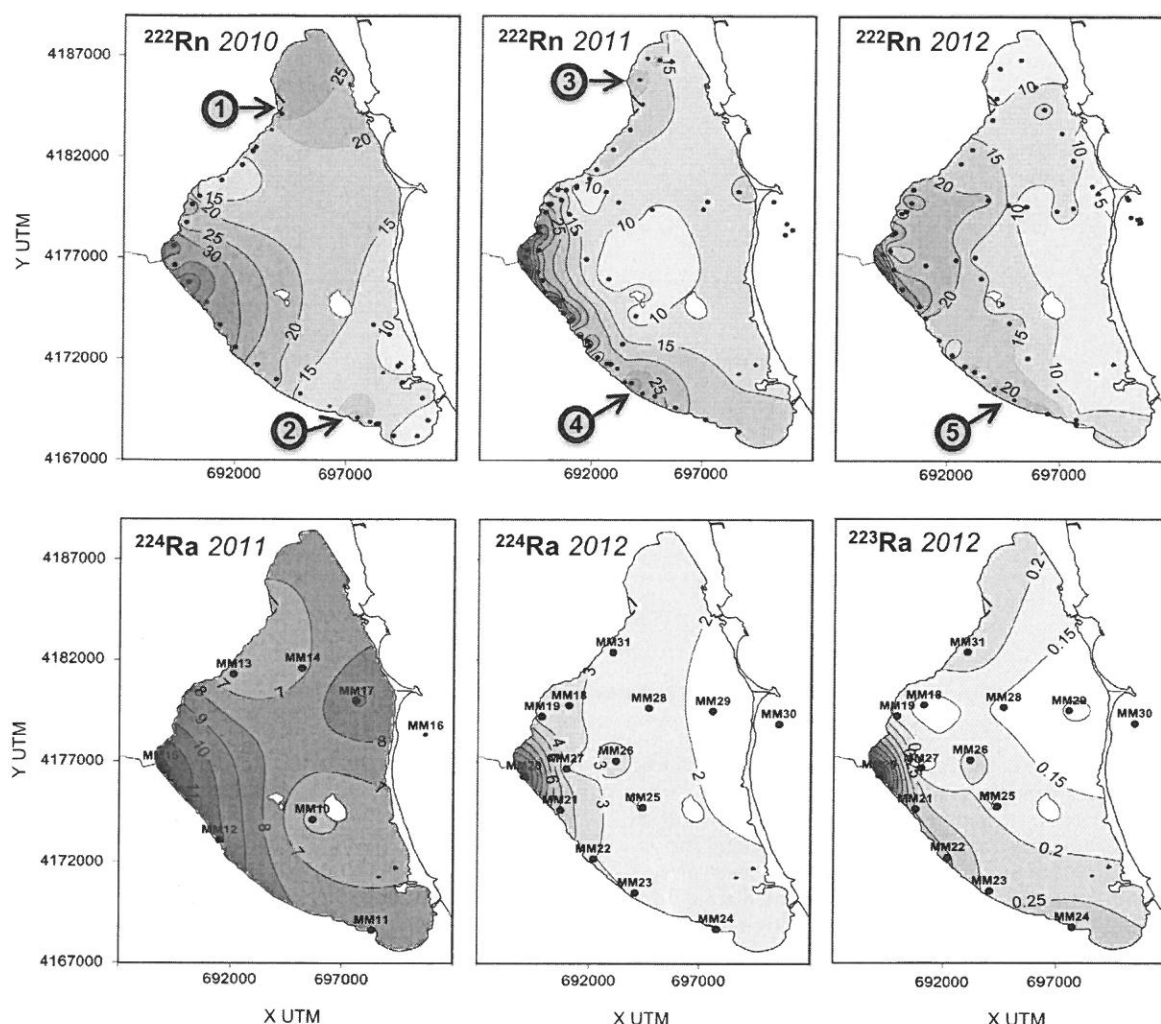


**Fig. 5.** Kriged maps of  $^{222}\text{Rn}$ ,  $^{224}\text{Ra}$  and  $^{223}\text{Ra}$  data from the lagoon ( $\text{Bq}/\text{m}^3$ ). Black dots are the location of each sample. Values for Mediterranean Sea samples are not indicated (refer to Table 3). Numbers 1–5 indicate areas distant from the Rambla that feature high radionuclide content.

#### 4.1.4. Sediments and porewater

The  $^{226}\text{Ra}$  activity of sediments ranged from 3.1 to 6.9  $\text{Bq}/\text{kg}$  (mean  $5.2 \pm 0.5 \text{ Bq}/\text{kg}$ ), and  $^{228}\text{Ra}$  from 3.4 to 11.3  $\text{Bq}/\text{kg}$  (mean  $6.6 \pm 1.1 \text{ Bq}/\text{kg}$ ). The equilibration experiments are used to provide a representative value of the activity of porewater just below the sediment–water interface. We obtained a mean activity of  $2600 \pm 400 \text{ Bq}/\text{m}^3$  for  $^{222}\text{Rn}$ ,  $150 \pm 60 \text{ Bq}/\text{m}^3$  for  $^{224}\text{Ra}$  and  $14.5 \pm 2.0 \text{ Bq}/\text{m}^3$  for  $^{223}\text{Ra}$ .

#### 4.2. Modeling of the currents

##### 4.2.1. Hydrodynamic calibration

Regarding the hydrodynamic calibration of the model, sea level data showed the best correlation ( $r=0.85$ ,  $\text{RMS}=1.2 \text{ cm}$ ). The speed currents recorded by the ADCPs in the lagoon in the days of the surveys were very low ( $<0.1 \text{ m/s}$ ) giving a correlation coefficient of 0.70 for current at 2 m above the bottom and 0.72 at 0.5 m above the bottom layer with RMS of 1.1 and 0.1  $\text{cm/s}$  respectively. However, higher speed currents showed higher correlation coefficient reproducing correctly the main hydrodynamic patterns.

##### 4.2.2. Radionuclide dispersion

The key steps of the output model for the dispersion of the  $^{222}\text{Rn}$  plume originated from a continuous Rambla discharge

during the 6 days before each campaign, including maximum southward and northward extent of the plume, are presented in Fig. 7. Graphical output of the model is available as online additional content. Basically, the modeled plume of the Rambla is driven northwards or southwards by wind currents, but always in a thick stripe (1 or 2 km max) along the coast. From highest represented values of  $60 \text{ Bq}/\text{m}^3$  ( $^{222}\text{Rn}$ ) and  $5 \text{ Bq}/\text{m}^3$  ( $^{224}\text{Ra}$ ) in the close surroundings of the discharge point, the plume of radionuclides from the Rambla reaches the mean lagoon value within a few kilometers, considering dispersion only.

In 2010,  $^{222}\text{Rn}$  and radium tracers started running in the model on 18/11 whereas data acquisition occurred on the 23 and 24/11. The modeled plume remained around the mouth until 20/11. After a slight displacement to the north on 21/11, and under the influence of westerly winds, the currents took the plume northwards and southwards over 3.5 km on 22 and 23/11, respectively. Finally, on 24/11, the currents quickly moved the southern part of the plume southwards down to a location between Los Urrutias and Los Nietos (7 km) while the northern part of the plume was dispersed.

In 2011, the injection of the tracer in the model started on 3/07. Very dynamic currents shifted the plume in the surroundings of the Rambla's mouth from 4 to 5/07 then continuously northwards up to Los Narejos (6 km distance) until the evening of 9/07. No

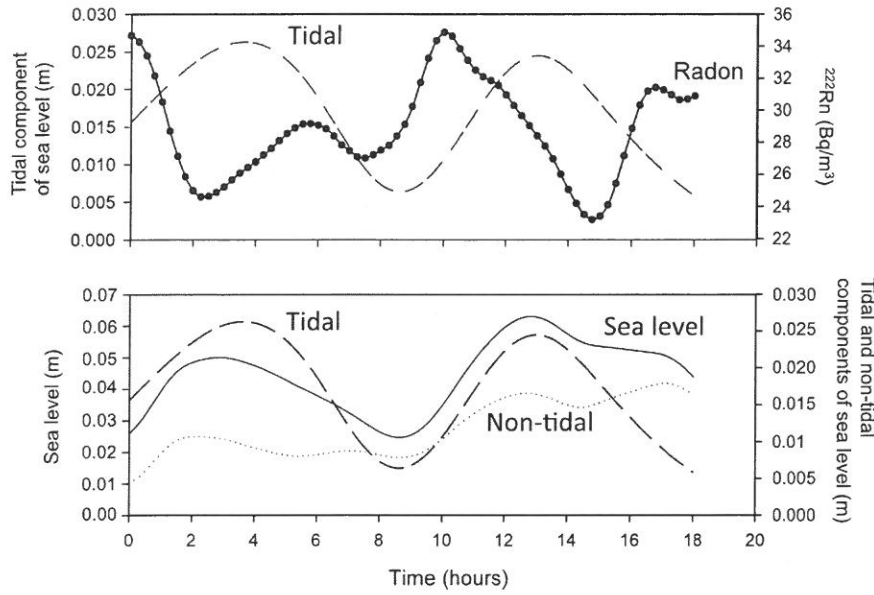


Fig. 6. Times series at the Los Urrutias harbour: sea level elevation (solid line), tidal component (dashed line), non-tidal component (dot line) and <sup>222</sup>Rn (black dots).

southwards displacement of the radionuclide plume was produced by the model for this survey.

In 2012, the injection started on 17/01. The plume first moved southwards in relation to strong northern winds reaching the village of Los Urrutias (5 km distance) on 19/01. As the speed currents decreased in mid-afternoon, a new plume was created around the mouth until 20/01 in mid-afternoon before moving northwards. From 21 to 24/01 evening, the newly originated plume was shifted northwards, reaching positions northwards from Los Narejos (7 km from the Rambla), while the first plume had remained immobile in the south since 19/01.

## 5. Discussion

### 5.1. Quantification of SGD

A clear excess of radionuclide was observed in the Mar Menor lagoon compared to the Mediterranean Sea. Therefore, a radionuclide flux balance between input flux ( $F_{input}$ ) and output flux ( $F_{output}$ ) of tracers is of high interest (e.g. Burnett et al., 2008; Mulligan and Charette, 2006; Gattacceca et al., 2011). Assuming a steady state, the excess of tracers is attributed to a SGD flux ( $F_{SGD}$ ) as follows (Eq. (1)):

$$F_{input} + F_{SGD} = F_{output} \quad (1)$$

The mass balance of the lagoon can therefore be performed using the following expressions for radon (Eq. (2)) and radium (Eq. (3)) isotopes:

$$(F_{in} + F_R + F_{diff} + F_{resuspension} + F_{prod}) + F_{SGD} = F_{decay} + F_{out} + F_{atm} \quad (2)$$

$$(F_{in} + F_R + F_{diff} + F_{resuspension} + F_{prod}) + F_{SGD} = F_{decay} + F_{out} \quad (3)$$

where input fluxes are the sum of the Mediterranean Sea inflow ( $F_{in}$ ), river inputs ( $F_R$ ), diffusive flux from sediments ( $F_{diff}$ ), flux from sediment resuspension ( $F_{resuspension}$ ) and radioactive production in water ( $F_{prod}$ ). Outputs are composed by the natural decay of the

tracers ( $F_{decay}$ ), the output flux to the Mediterranean Sea ( $F_{out}$ ) and the radon atmospheric flux to the atmosphere ( $F_{atm}$ ).

These different parameters are detailed and discussed in the following sections and summarized in Table 4 to achieve the radionuclide budgets in July 2011 and January 2012. The uncertainties associated to all radionuclides fluxes used in the budgets are calculated at  $1\sigma$ . Special attention was paid to surface water and groundwater end-members, in addition to the input from resuspended sediments, not always considered in details in most studies.

#### 5.1.1. Assessment of <sup>222</sup>Rn and radium fluxes

**5.1.1.1. Radon atmospheric flux ( $F_{atm}$ ).** The radon flux across the air–water interface ( $J_{atm}$ , in Bq/m<sup>2</sup>/d) is generally calculated as (Eqs. (4) and (5)):

$$F_{atm} = J_{atm} \text{ Surface}_{MM} \quad (4)$$

with

$$J_{atm} = k(C_w - \alpha C_{air}) \quad (5)$$

where  $\text{Surface}_{MM}$  is the surface area of the Mar Menor lagoon (in m<sup>2</sup>),  $C_w$  and  $C_{air}$  are the radon activities in water and air, respectively (Bq/m<sup>3</sup>).  $\alpha$  is the Ostwald's solubility coefficient (dimensionless), i.e. the water–air partition coefficient of radon. It depends on both temperature and salinity and was calculated according to Schubert et al. (2012). The variable  $k$  is the gas transfer velocity (cm/h), which depends on kinematic viscosity, molecular diffusion and turbulence (principally due to wind speed). We use the empirical relationship between  $k$  and wind speed by MacIntyre et al. (1995) and Turner et al. (1996), as follows (Eqs. (6) and (7)):

$$\text{for } u_{10} \leq 3.6 \text{ m/s : } k = 0.45 u_{10}^{1.6} (S_c/600)^{-2/3} \quad (6)$$

$$\text{for } u_{10} > 3.6 \text{ m/s : } k = 0.45 u_{10}^{1.6} (S_c/600)^{-0.5} \quad (7)$$

where  $u_{10}$  is the wind speed at 10 m height (m/s) and  $S_c$  is the Schmidt number for radon, i.e. the ratio of the kinematic viscosity to the molecular diffusion coefficient, calculated in the conditions of salinity and temperature.

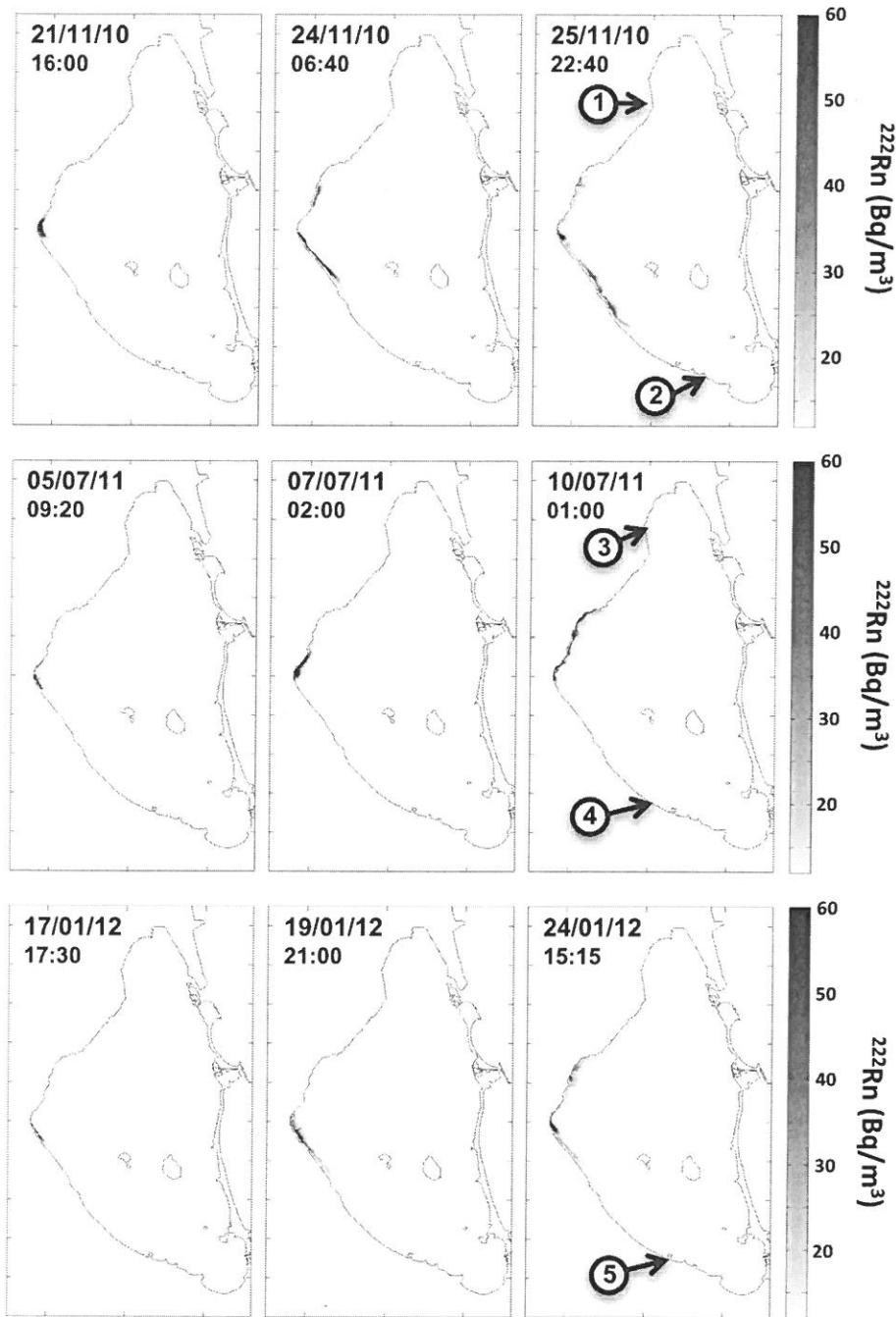


Fig. 7. Simulation of the extreme southwards and northwards displacement of the simulated Rambla del Albujón  $^{222}\text{Rn}$  plume during the 6 days before the 2010, 2011 and 2012 sampling campaigns. Areas of high measured radionuclide activity out of the reach of this plume are indicated by numbers.

The different conditions for wind speed and water temperature between July (4.0 m/s and 28.9 °C) and January surveys (1.0 m/s and 12.8 °C) lead to important changes in the calculated atmospheric flux. The radon atmospheric loss was  $12.3 \pm 1.4 \text{ Bq/m}^2/\text{d}$  in July and  $0.7 \pm 0.1 \text{ Bq/m}^2/\text{d}$  in January.

**5.1.1.2. Diffusive flux from sediments ( $F_{\text{diff}}$ ).** The equilibration experiments allowed estimating the diffusive flux from the sediment  $F_{\text{diff}}$  for each radionuclide. This flux refers here to the process of diffusion through activity gradient between porewater just below the surface of the sediment and the water column above it (it does not correspond to small-advective process, included in RSGD).

The diffusive flux  $F_{\text{diff}}$  is obtained from the specific diffusive flux  $J_{\text{diff}}$  as follows:

$$F_{\text{diff}} = J_{\text{diff}} \text{ Surface}_{\text{MM}} \quad (8)$$

$J_{\text{diff}}$  is calculated according to Martens et al. (1980) assuming steady state conditions and no advective transport (Eq. (9)):

$$J_{\text{diff}} = \sqrt{\lambda D_s} (C_{\text{eq}} - C_0) \quad (9)$$

where  $J_{\text{diff}}$  is expressed in  $\text{Bq/m}^2/\text{min}$ ,  $\lambda$  is the decay constant ( $\text{d}^{-1}$ ),  $D_s$  is the effective radon or radium diffusion coefficient in sediments ( $\text{m}^2/\text{d}$ ),  $C_{\text{eq}}$  is the activity in porewater (estimated from the

**Table 4**Definition and values for each term of the Ra–Rn mass balance. Uncertainties on all radionuclides fluxes are  $1\sigma$ .

Definition	July 2011 $^{222}\text{Rn}$	July 2011 $^{224}\text{Ra}$	January 2012 $^{222}\text{Rn}$	January 2012 $^{224}\text{Ra}$	January 2012 $^{223}\text{Ra}$	Units
<b>Inputs</b>						
$F_{\text{in}}$ : input flux from the Mediterranean Sea ( $\text{activity}_{\text{SW}} \cdot Q_{\text{in}}$ )	$2.0 \pm 0.7 \cdot 10^7$	$6.4 \pm 3.0 \cdot 10^6$	$1.4 \pm 0.3 \cdot 10^7$	$1.8 \pm 0.2 \cdot 10^6$	$2.1 \pm 0.8 \cdot 10^5$	Bq/d
Activity <sub>SW</sub> : tracer ( $^{222}\text{Rn}$ , $^{224}\text{Ra}$ or $^{223}\text{Ra}$ ) activity in the Mediterranean Sea	2.9	1.2	2.6	0.34	0.04	Bq/m <sup>3</sup>
$Q_{\text{in}}$ : water inflow from the Med. Sea into Mar Menor	$5.4 \cdot 10^6$	$5.4 \cdot 10^6$	$5.4 \cdot 10^6$	$5.4 \cdot 10^6$	$5.4 \cdot 10^6$	m <sup>3</sup> /d
$F_{\text{R}}$ : input flux from rivers ( $\text{activity}_{\text{R}} \cdot Q_{\text{R}}$ )	$5.7 \pm 1.0 \cdot 10^7$	$1.8 \pm 0.4 \cdot 10^6$	$8.2 \pm 1.0 \cdot 10^7$	$3.1 \pm 0.4 \cdot 10^6$	$1.5 \pm 0.2 \cdot 10^5$	Bq/d
Activity <sub>R</sub> : tracer activity in rivers (Rambla)	2000	64	2900	108	5.2	Bq/m <sup>3</sup>
$Q_{\text{R}}$ : water inflow from rivers into Mar Menor	$2.8 \cdot 10^4$	$2.8 \cdot 10^4$	$2.8 \cdot 10^4$	$2.8 \cdot 10^4$	$2.8 \cdot 10^4$	m <sup>3</sup> /d
$F_{\text{diff}}$ : Diffusive flux from sediment ( $J_{\text{diff}} \cdot S_{\text{MM}}$ )	$1.1 \pm 0.2 \cdot 10^9$	$5.2 \pm 2.0 \cdot 10^7$	$9.2 \pm 1.0 \cdot 10^8$	$4.4 \pm 2.0 \cdot 10^7$	$2.5 \pm 0.4 \cdot 10^6$	Bq/d
$J_{\text{diff}}$ : see in the text	8.9	0.40	7.2	0.34	0.019	Bq/m <sup>2</sup> /d
$S_{\text{MM}}$ : surface area of Mar Menor	$1.3 \cdot 10^8$	$1.3 \cdot 10^8$	$1.3 \cdot 10^8$	$1.3 \cdot 10^8$	$1.3 \cdot 10^8$	m <sup>2</sup>
$F_{\text{resuspension}}$ : input of tracer from resuspended sediment	$4.5 \cdot 10^4$	$2.7 \cdot 10^4$	0	0	0	Bq/d
$F_{\text{prod}}$ : production from parent in water ( $\lambda \cdot \text{activity}_{\text{P}}$ )	$2.3 \pm 0.3 \cdot 10^8$	$6.2 \pm 1.0 \cdot 10^7$	$2.3 \pm 0.3 \cdot 10^8$	$6.2 \pm 1.0 \cdot 10^7$		Bq/d
Activity <sub>P</sub> : activity of the parent in water	2.1	0.54	2.1	0.54	Negligible	Bq/m <sup>3</sup>
Total inputs	$1.5 \pm 0.2 \cdot 10^9$	$1.2 \pm 0.3 \cdot 10^8$	$1.3 \pm 0.1 \cdot 10^9$	$1.1 \pm 0.2 \cdot 10^8$	$2.8 \pm 0.4 \cdot 10^6$	Bq/d
<b>Outputs</b>						
$F_{\text{decay}}$ : decay of tracers in the studied volume ( $\text{activity}_{\text{MM}} \cdot V_{\text{MM}} \cdot \lambda$ )	$1.4 \pm 0.1 \cdot 10^9$	$8.7 \pm 0.9 \cdot 10^8$	$1.4 \pm 0.1 \cdot 10^9$	$2.9 \pm 0.2 \cdot 10^8$	$7.3 \pm 2.0 \cdot 10^6$	Bq/d
Activity <sub>MM</sub> : mean activity of the tracer in Mar Menor	12.6	7.6	13.1	2.5	0.2	Bq/m <sup>3</sup>
$V_{\text{MM}}$ : water volume in Mar Menor	$6.1 \cdot 10^8$	$6.1 \cdot 10^8$	$6.1 \cdot 10^8$	$6.1 \cdot 10^8$	$6.1 \cdot 10^8$	m <sup>3</sup>
$\lambda$ : decay constant of the tracer	$1.81 \cdot 10^{-1}$	$1.89 \cdot 10^{-1}$	$1.81 \cdot 10^{-1}$	$1.89 \cdot 10^{-1}$	$6.06 \cdot 10^{-2}$	d <sup>-1</sup>
$F_{\text{out}}$ : output flux to the Mediterranean Sea ( $\text{activity}_{\text{MM}} \cdot Q_{\text{out}}$ )	$3.7 \pm 0.5 \cdot 10^7$	$2.2 \pm 0.3 \cdot 10^7$	$3.9 \pm 0.5 \cdot 10^7$	$7.4 \pm 0.9 \cdot 10^6$	$5.9 \pm 0.8 \cdot 10^5$	Bq/d
$Q_{\text{out}}$ : water outflow from Mar Menor to the Med. Sea	$2.9 \cdot 10^6$	$2.9 \cdot 10^6$	$2.9 \cdot 10^6$	$2.9 \cdot 10^6$	$2.9 \cdot 10^6$	m <sup>3</sup> /d
$F_{\text{atm}}$ : Radon atmospheric flux to the atmosphere ( $J_{\text{atm}} \cdot S_{\text{MM}}$ )	$1.6 \pm 0.2 \cdot 10^9$		$9.2 \pm 1.0 \cdot 10^7$			Bq/d
$J_{\text{atm}}$ : radon atmospheric loss to the atmosphere per unit area per day	12.3		0.7			
Total outputs	$3.0 \pm 0.2 \cdot 10^9$	$8.9 \pm 0.9 \cdot 10^8$	$1.6 \pm 0.1 \cdot 10^9$	$2.9 \pm 0.2 \cdot 10^8$	$7.9 \pm 2.0 \cdot 10^6$	Bq/d
$F_{\text{SGD}}$ : Submarine groundwater discharge flux of tracers, estimated by difference between output terms and input terms	$1.6 \pm 0.3 \cdot 10^9$	$7.7 \pm 0.9 \cdot 10^8$	$3.2 \pm 2.0 \cdot 10^8$	$1.8 \pm 0.3 \cdot 10^8$	$5.1 \pm 2.0 \cdot 10^6$	Bq/d
Activity <sub>GW</sub> : tracer activity in groundwater endmember	2600	150	2600	150	14.5	Bq/m <sup>3</sup>
SGD water flux: $F_{\text{SGD}}/\text{activity}_{\text{GW}}$	$2.2 \pm 0.5 \cdot 10^8$	$1.9 \pm 0.8 \cdot 10^9$	$4.5 \pm 3.0 \cdot 10^7$	$4.4 \pm 2.0 \cdot 10^8$	$1.3 \pm 0.7 \cdot 10^8$	m <sup>3</sup> /y

equilibration experiments; Bq/m<sup>3</sup>) and  $C_0$  is the activity in the overlying water column during the field campaign (Bq/m<sup>3</sup>). The effective radon diffusion coefficient  $D_s$  was calculated according to Ullman and Aller (1981) ( $D_s = P \cdot D_0$ ) with a porosity  $P$  equal to 0.5 and the molecular diffusion coefficient  $D_0$  is calculated according to Peng et al. (1974) using field temperature reported in Table 3.  $D_s$  were  $6.3 \cdot 10^{-5}$  and  $4.2 \cdot 10^{-5}$  m<sup>2</sup>/d for July and January respectively. For radium,  $D_s$  was extrapolated from the data of Li and Gregory (1974) and were  $8.4 \cdot 10^{-5}$  and  $5.6 \cdot 10^{-5}$  m<sup>2</sup>/d for July and January respectively. The equilibration experiments returned mean porewater radon and radium activities (see Section 4.1.4) in agreement with the range found in the literature (Beck et al., 2007; Michael et al., 2011; Moore et al., 2011; Kluge et al., 2012; Cockenpot et al., 2015).

The corresponding mean specific radon diffusive fluxes estimated for July and January were  $8.8 \pm 1.4$  and  $7.1 \pm 1.1$  Bq/m<sup>2</sup>/d. These values can be compared with the one calculated using the empirical relationship of Burnett et al. (2003):

$$J_{\text{diff}} = 0.495^{226}\text{Ra} + 0.303 \quad (10)$$

where  $^{226}\text{Ra}$  is the activity of the sediment (Bq/kg). Although much simpler, this second method provided here similar results (mean of  $2.9 \pm 1.0$  Bq/m<sup>2</sup>/d) which strengthens the reliability of the approach and shows that the choice of the method has a limited impact on the final balance of the lagoon. The values calculated according to the equilibrium method were used for the radionuclide mass balance.

The specific diffusive flux calculated for  $^{224}\text{Ra}$  was very similar for July and January (mean of  $0.37 \pm 0.03$ ) and  $0.019 \pm 0.003$  Bq/m<sup>2</sup>/d for  $^{223}\text{Ra}$  in January. They are similar to those obtained by Garcia-Solsona et al. (2008) in the Venice lagoon (0.53 and

0.018 Bq/m<sup>2</sup>/d for  $^{224}\text{Ra}$  and  $^{223}\text{Ra}$  respectively) and Beck et al. (2007) in the Jamaica Bay (0.47 Bq/m<sup>2</sup>/d and 0.019 Bq/m<sup>2</sup>/d for  $^{224}\text{Ra}$  and  $^{223}\text{Ra}$  respectively) whose approach based on whole core incubations included both true diffusive and bio-diffusive and bio-irrigation fluxes.

**5.1.1.3. Radioactive decay ( $F_{\text{decay}}$ ).** Radioactive decay ( $F_{\text{decay}}$ ) was calculated using the following expression (Eq. (11)):

$$F_{\text{decay}} = \text{activity}_{\text{MM}} V_{\text{MM}} \quad (11)$$

where activity<sub>MM</sub> is the mean activity of the tracer in Mar Menor and  $V_{\text{MM}}$  the volume of Mar Menor. As  $F_{\text{decay}}$  generally has a strong influence on the total budget, the mean activity used for the calculation needs to be very accurate. In order not to overestimate the weight of the larger amount of data collected along the coastline, a 3D interpolation of the data was performed by kriging with 100 m/100 m cells taking in account the water depth of each one. As an example, in 2012, the arithmetic mean gives a mean  $^{224}\text{Ra}$  activity<sub>MM</sub> of 3.7 Bq/m<sup>3</sup> compared to 2.5 Bq/m<sup>3</sup> with the interpolation.

$F_{\text{decay}}$  for  $^{222}\text{Rn}$  was similar in July and January ( $1.4 \pm 0.1 \cdot 10^9$  Bq/d, Table 3). Regarding  $^{224}\text{Ra}$ , the mean value was almost three times higher in July ( $2.9 \pm 0.2 \cdot 10^8$  and  $8.7 \pm 0.9 \cdot 10^8$  Bq/d for January and July respectively, Table 3).

**5.1.1.4. Inputs from resuspended sediment ( $F_{\text{resuspension}}$ ).** Resuspension of sediment can add radium to the water column by release of Ra-enriched porewater plus desorption of Ra from resuspended sediments. Assuming that turbidity is only due to daily resuspension, the average turbidity measured in July (1.1 NTU, i.e.  $\approx 0.07$  mg/L) provides a maximum estimation of the total resuspended sediment



of  $3.26 \cdot 10^4$  kg/d. Combining this result with the density of sediment ( $2350 \text{ kg/m}^3$ ) and the calculated porosity (0.5), we estimated a maximum amount of porewater daily released in the Mar Menor of  $17.5 \text{ m}^3$ , corresponding to  $2600 \text{ Bq}$  of  $^{224}\text{Ra}$  (using a  $^{224}\text{Ra}$  activity in porewater of  $150 \text{ Bq/m}^3$ ). The amount of  $^{224}\text{Ra}$  desorbed from resuspended sediments is calculated from the mean concentration of  $^{228}\text{Ra}$  in sediments ( $6.6 \text{ Bq/kg}$ ) and considering that 7% of  $^{224}\text{Ra}$  can be desorbed (Moore et al., 2011). This lead to a value of  $1.9 \cdot 10^4 \text{ Bq}$ . Summing both sources gave a maximum input of  $^{224}\text{Ra}$  by resuspension of  $2.7 \cdot 10^4 \text{ Bq/d}$ . This value is two orders of magnitude lower than that obtained in Venice lagoon ( $3.3 \cdot 10^6 \text{ Bq/d}$ ) by Garcia-Solsona et al. (2008) and in Jamaica bay ( $3.8 \cdot 10^6 \text{ Bq/d}$ ) by Beck et al. (2007), a difference directly due to our lower turbidity (up to  $1 \text{ mg/L}$  in Venice and  $20 \text{ mg/L}$  in Jamaica Bay).

For  $^{222}\text{Rn}$ , which is not adsorbed onto sediments, the input from resuspension is caused only by the release from porewater. The  $^{222}\text{Rn}$  activity of  $2600 \text{ Bq/m}^3$  estimated for this porewater gives a maximum input of  $4.5 \cdot 10^4 \text{ Bq/d}$ . In January 2012, as no wind affected the survey significantly (turbidity close to zero), radium and radon fluxes from sediments resuspension are neglected.

**5.1.1.5. Production by parents decay ( $F_{\text{prod}}$ ).** The activity of the tracer parents,  $^{226}\text{Ra}$ ,  $^{228}\text{Th}$ , and  $^{227}\text{Ac}$  in water in the Mar Menor were measured and multiplied by the radioactive decay constant of their respective daughter to estimate the production input in the water column. The production was  $2.3 \pm 0.3 \cdot 10^8 \text{ Bq/d}$  and  $6.2 \pm 1.0 \cdot 10^7 \text{ Bq/d}$  for  $^{222}\text{Rn}$  and  $^{224}\text{Ra}$ , respectively, and negligible for  $^{223}\text{Ra}$ .

**5.1.1.6. Inputs from the Rambla ( $F_r$ ).** According to the mean discharge rate and radionuclide activities (see Section 4.1.2), the fluxes from the Rambla to the lagoon in July 2011 and January 2012, respectively, are the following:  $5.7 \pm 1.0 \cdot 10^7$  and  $8.2 \pm 1.0 \cdot 10^7 \text{ Bq/d}$  for  $^{222}\text{Rn}$ ;  $1.8 \pm 0.4 \cdot 10^6$  and  $3.1 \pm 0.4 \cdot 10^6 \text{ Bq/d}$  for  $^{224}\text{Ra}$ . Regarding  $^{223}\text{Ra}$ , the value for January 2012 is  $1.5 \pm 0.2 \cdot 10^5 \text{ Bq/d}$ .

The high changes in  $^{222}\text{Rn}$  activities for R1, R2 or R3 surface waters (Table 2) are linked to the high reactivity of the watershed to artificial discharges. Not all discharge rates could be measured and the presence of water along the watershed is discontinuous, therefore, a quantitative assessment of the contribution of each tributary was difficult to assess. Nonetheless, the good correlation between  $^{222}\text{Rn}$  activities and discharge for R1 and R3 from 20 to 24 January 2012 and the very short distance between these two points tends to demonstrate that R3 potentially has a major and direct impact on the  $^{222}\text{Rn}$  signal discharged by R1 into Mar Menor. The same interpretation is suggested for the extreme R3 and R1  $^{222}\text{Rn}$  activities (close to  $12,000 \text{ Bq/m}^3$  for R1) measured on 10 July 2011, although discharge was not quantified.

R3 presents the highest measured  $^{222}\text{Rn}$  activities (close to  $18,000 \text{ Bq/m}^3$ ). Nonetheless, our dedicated sampling showed that reverse osmosis process does not modify consistently the  $^{222}\text{Rn}$  activities between pumped groundwater, final product and brines. Therefore,  $^{222}\text{Rn}$  does not provide additional criteria to identify the origin of this undocumented emissary. By contrast, the electrical conductivity of R3, as well as  $^{222}\text{Rn}$  activity, that are the highest of all tributaries and also higher than groundwater samples, highlights the notable contribution of brines from desalinated water.

The release from the Los Alcázares sewage water treatment plant was found to dilute the  $^{222}\text{Rn}$  signal in the river, from 2200 upstream to  $900 \text{ Bq/m}^3$  downstream (samples 5 and 6 in Table 2, not located on the map). It therefore does not act as a notable source of  $^{222}\text{Rn}$  for the watershed. Low activities in wastewater were also found for radium by Beck et al. (2007).

### 5.1.2. SGD end-member

Defining the radionuclide activities associated with FSGD and RSGD inputs and their relative contribution is probably the most sensitive step for SGD quantification (e.g. Mulligan and Charette, 2006; Weinstein et al., 2007). Although some authors attempted to separate these sub-components geochemically (e.g. McCoy et al., 2007; Taniguchi et al., 2006; Santos et al., 2012) current investigations usually define one unique integrated value as representative for all SGD fluxes.

As described in details by Simonneau (1973) in her study of the sedimentary infill of the lagoon and later confirmed by seismic reflection profiles (IGME, 1983), the Quaternary aquifer below Mar Menor is fully covered by a sedimentary layer, close to  $10 \text{ m}$  thick. These sediments were deposited in the Quaternary during a series of marine transgressions and regressions, whose limits slightly exceed the present western limits of the lagoon (Simonneau, 1973). As a consequence, the sediment cover of the lagoon and the Quaternary aquifer represent two distinct lithological entities.

This site-specific feature leads us to consider the sediment cover of the lagoon as an intermediary compartment that collects and mixes inputs from both continental groundwater and recirculated seawater before their release through SGD to the lagoon. Depending on their respective residence time in the sediment cover, their radionuclide composition may evolve by the combined effects of radiogenic decay and equilibration. Therefore, assessing the residence time of waters in the sediments may provide insightful information to define the composition of the resulting discharging water.

The residence time of FSGD continental groundwater in the sediments can be calculated with local hydrodynamic data, assuming a continuous flow between the Quaternary aquifer and the porous sediment underlying the lagoon. The velocity of continental groundwater ( $v_{\text{GW}}$ ) is provided by the following expression (Eq. (12)), where  $k$  is the hydraulic conductivity,  $n_e$  is the effective porosity and  $i$  is the hydraulic gradient:

$$v_{\text{GW}} = \frac{ki}{n_e} \quad (12)$$

Considering respective values of  $1.5 \text{ m/d}$ , 30% (according to Senent et al., 2009 and Jiménez-Martínez et al., 2012) and 5 per mil (IEA, 2011), the mean velocity of continental groundwater in the Quaternary aquifer is  $2.5 \text{ cm per day}$  ( $9.1 \text{ m/y}$ ). As the average thickness of the sediment cover is close to ten meters (Simonneau, 1973), and assuming a similar order of magnitude for the velocity of the continental groundwater inside the sediment cover, the residence time of continental groundwater in the sediments lies around 1 year.

The evolution of the radionuclide activities of both continental groundwater and recirculated saline water entering the sediment with residence time can be described by combining radioactive decay and production into one global equation (Eq. (13), derived from Bateman's expression for  $^{222}\text{Rn}$ ,  $^{224}\text{Ra}$  and  $^{223}\text{Ra}$ ):

$$A(t) = A_0 \exp^{-\lambda t} + A_{\text{porewater}}(1 - \exp^{-\lambda t}) \quad (13)$$

where  $A(t)$  is the radionuclide activity of continental groundwater or recirculated saline water at a given residence time  $t$  inside the sediments,  $A_0$  is the initial activity of this water and  $A_{\text{porewater}}$  is the activity of the radionuclide ( $^{222}\text{Rn}$ ,  $^{224}\text{Ra}$  or  $^{223}\text{Ra}$ ) in porewater at secular equilibrium with their parent (obtained from Section 4.1.4).

Fig. 8 illustrates the respective evolutions of  $^{222}\text{Rn}$  from continental groundwater (highest measured activity, sample G from July 2012) and from recirculated saline water inside the sediment cover, together with the  $^{222}\text{Rn}$  activity of porewater at

secular equilibrium. It reveals that less than 30 days are required for the highest activity measured in continental groundwater (radionuclide-rich) to reach the order of magnitude of porewater. It would only require a tenth of days in the case of the lowest activity from continental groundwater, lower than the one of porewater at secular equilibrium (sample A1 from July 2011, not illustrated). As these values are 10 to 30 times lower than the above-calculated residence time for continental groundwater inside the sediment cover, the activity of porewater is the most representative of the FSGD component.

Similarly, Fig. 8 shows that the  $^{222}\text{Rn}$  activity of recirculated saline water, initially radionuclide-poor, needs a tenth of days to attain the one of porewater. As the actual residence time of recirculated saline water is expected to be lower than the equilibration time (e.g. Santos et al., 2009b,c), the actual value for the RSGD component would most probably be lower. Therefore, the  $^{222}\text{Rn}$  activity of porewater represents a maximum value for the RSGD component. The same conclusions regarding both RSGD and FSGD are found for  $^{224}\text{Ra}$  and  $^{223}\text{Ra}$ .

A maximum integrated value for the radionuclide composition of SGD is therefore given:  $2600 \pm 400 \text{ Bq/m}^3$  for  $^{222}\text{Rn}$ ,  $14.5 \pm 2.0 \text{ Bq/m}^3$  for  $^{223}\text{Ra}$  and  $150 \pm 60 \text{ Bq/m}^3$  for  $^{224}\text{Ra}$ . The actual values might be slightly lower and changing through time, due to the highly variable proportion of FSGD and RSGD in total SGD (e.g. Weinstein et al., 2007) and to the expected low residence time of recirculated saline water. Considering the composition of groundwater sampled from piezometers as representative of the SGD composition (e.g. Gattacceca et al., 2011; Rodellas et al., 2012) would have most probably led, in this specific case, to a strong underestimation of SGD fluxes.

### 5.1.3. Radionuclide mass balance

Ra and Rn mass balances of the lagoon (Table 4) were performed paying special attention to the atmospheric evasion and resuspension inputs, clearly different between summer (2011) and winter (2012) due to various wind and temperature conditions.

The calculated excess fluxes for  $^{222}\text{Rn}$  are 5 times higher in July 2011 than in January 2012 with  $16 \pm 3 \cdot 10^8$  and  $3.2 \pm 2 \cdot 10^8 \text{ Bq/d}$  respectively (Table 4). These values are 4–28 times higher than the influx from the Rambla del Albujón. The main fluxes influencing the radon balance are the decay ( $F_{\text{decay}}$ ), the atmospheric fluxes ( $F_{\text{atm}}$ ) together with the diffusive flux from sediments ( $F_{\text{diff}}$ ), whereas resuspension has a very low impact (five orders of magnitude less than  $F_{\text{decay}}$ ). The impact of other fluxes that were found to change between the two dates (sediment diffusion and rivers) is

one or two orders of magnitude lower. As wind speed and temperature have no control on the SGD process but only on total stock of  $^{222}\text{Rn}$  in the lagoon, the SGD flux calculated for no-wind conditions (January 2012) is less affected by external processes.

The calculated SGD fluxes for  $^{224}\text{Ra}$  in Summer 2011 and Winter 2012 vary by a factor of 4 ( $7.7 \pm 0.9$  and  $1.8 \pm 0.3 \cdot 10^8 \text{ Bq/d}$  respectively, see Table 4). The main term in this calculation is the radioactive decay ( $F_{\text{decay}}$ ), followed by the in-situ production from radioactive parents ( $F_{\text{prod}}$ ) and the diffusive flux from sediments ( $F_{\text{diff}}$ ). The difference in the SGD water flux between the two dates is mostly explained by the lower mean  $^{224}\text{Ra}$  value in the lagoon in 2012 that induced lower decay. The other parameters that were notably different between the campaigns actually have a negligible impact on the  $^{224}\text{Ra}$  balance: twice  $^{224}\text{Ra}$  activity in the Rambla del Albujón ( $+1.5 \cdot 10^6 \text{ Bq/d}$ ), lower exchanges with Mediterranean Sea ( $-2.5$  and  $-5.3 \cdot 10^6 \text{ Bq/d}$  for input and output, respectively). As well as for  $^{222}\text{Rn}$ , the contribution of resuspended sediments in 2011 has a very limited impact on the balance ( $2.7 \cdot 10^4 \text{ Bq/d}$ ). Similarly, SGD is a more important source of radium than the Rambla del Albujón (Table 4): from one order of magnitude ( $^{223}\text{Ra}$ ) to two orders of magnitude ( $^{224}\text{Ra}$ ).

Garcia-Orellana et al. (2014) recently showed that bioirrigation fluxes could increase the  $^{224}\text{Ra}$  input to the mass balance. Such fluxes are enhanced with the activity of the benthic fauna, i.e. generally in summer. They were not evaluated here but cannot be ruled out. In particular, bioirrigation could explain the difference between SGD fluxes estimated in summer and winter.

According to the  $^{222}\text{Rn}$  mass balance of the lagoon, SGD fluxes of water of  $2.2 \pm 0.5$  and  $0.5 \pm 0.3 \cdot 10^8 \text{ m}^3/\text{y}$  are obtained for summer and winter season respectively. SGD fluxes of water calculated from  $^{224}\text{Ra}$  are  $19 \pm 8$  and  $4.4 \pm 2 \cdot 10^8 \text{ m}^3/\text{y}$ , and the one calculated from  $^{223}\text{Ra}$  is  $1.3 \pm 0.6 \cdot 10^8 \text{ m}^3/\text{y}$ .

### 5.1.4. Fraction of continental water in total SGD

As demonstrated in Section 5.1.2, the sediment cover acts as mixing compartment for the RSGD and FSGD radionuclide signals. Indeed, the difficulty in distinguishing between both components of SGD solely based on radionuclide activity was observed in numerous studies (e.g. Mulligan and Charette, 2006; Weinstein et al., 2007). The objective of the present section is to provide an insight on the relative contribution of FSGD and RSGD in total SGD by combining several approaches.

FSGD is usually controlled by inland groundwater hydrodynamics (Santos et al., 2012), whereas the main driving force of RSGD is generally considered to be tidal (recirculation between high and low tides) or wave pumping (Weinstein et al., 2007). Because of

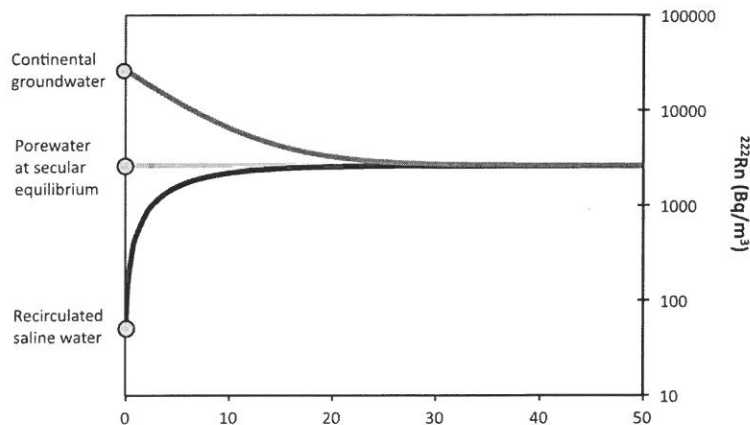


Fig. 8. Evolution of the  $^{222}\text{Rn}$  activity of continental groundwater (sample G from July 2012) and recirculated saline water for a given residence time inside the sediment cover. The activity of porewater at secular equilibrium is also indicated.

the limited amplitude of sea-level variations (a few centimeters), and the very narrow width of the shore (a few meters), tidal pumping was expected to have limited influence on the SGD fluxes through RSGD to Mar Menor. We extracted the tidal component of the elevation of sea level during the continuous sampling in the Los Urrutias port through harmonic tide analysis (Emery and Thomson, 2001). Surprisingly, a significant negative correlation ( $r = -0.44$ ;  $n = 73$ ,  $P < 0.001$ ) was found between the tidal level and the radon activity (Fig. 6). A cross correlation between these factors even increased the correlation coefficient up to  $-0.63$  for a time lag of 75 min. These data suggest that tidal forcing explains 40% of the variance between radon activity and tide with a delay of 1.25 h. It therefore influences notably the SGD fluxes, as previously suggested (e.g. Weinstein et al., 2007), most probably through a modified proportion of FSGD and RSGD (e.g. Santos et al., 2009a).

Non-tidal sea level variations have a similar range of variations (0.03 m) and might also play a role as a driver of SGD. Nonetheless, they showed a non-significant correlation ( $r = -0.08$ ,  $n = 73$ ,  $P < 0.50$ ), probably due to their no-cyclical behavior at such spatio-temporal scale (Fig. 6). Indeed, non-tidal sea level variations are mainly controlled by atmospheric pressure and winds. It must be noted that bioturbation might be associated to another kind of advective process (Stieglitz et al., 2013), not considered here.

We compared our radionuclide-integrated estimates with the Darcy's law and hydrogeological modeling (Smith, 2004). Taking the same parameters as used in Section 5.1.2, with a hydraulic conductivity of 1.5 m/d (60 m of mean saturated thickness), a hydraulic gradient of 5‰ and a total length of discharge between the Quaternary aquifer and the lagoon of 29.6 km, the Darcy's equation provides a FSGD of  $5 \cdot 10^6 \text{ m}^3/\text{y}$ . A mathematical model of the Quaternary aquifer with the same parameters and calibrated on transmissivity provided a FSGD of  $7.6 \cdot 10^6 \text{ m}^3/\text{y}$  (Senent et al., 2009). Comparing this last estimate with the integrated ones obtained with radionuclides (Table 4), FSGD would represent between 2% (in July 2011) and 8% (in January 2012) of total SGD. Martínez-Alvarez et al. (2011) used a global salt balance in the lagoon and deduced a FSGD of  $21 \cdot 10^6 \text{ m}^3/\text{y}$ . Comparing the FSGD value from Martínez-Alvarez et al. (2011) to the total SGD obtained by radionuclides, the ratio would increase up to 5% (in July 2011) and 23% (in January 2012). These results are similar to calculations in other locations: around 4% for Santos et al. (2009c) and below 80% for Mulligan and Charette (2006).

## 5.2. Location of radionuclide inputs

The model provides information on the shape of the plume produced by dispersion of the discharge of the Rambla in the lagoon. In the close surroundings of the mouth, the elevated activities ( $60 \text{ Bq/m}^3$  for  $^{222}\text{Rn}$  and  $5 \text{ Bq/m}^3$  for  $^{224}\text{Ra}$ ) are supported by the recorded  $^{222}\text{Rn}$  and  $^{224}\text{Ra}$  activities. Nonetheless, in this specific area, such high activities combined with the complex hydrodynamics do not allow a precise differentiation between SGD and surface water inputs.

Farther from the Rambla output, in locations not reached by the plume in the previous 6 days (Fig. 7), the highest measured  $^{222}\text{Rn}$  values (points 1, 2, 3, 4, 5; Fig. 5) cannot be explained by the contribution of the plume in this time-lapse. To justify the measured values, a previous plume that would have reached this area earlier than the 6 days of modeling would have needed the following theoretical initial radon activity ( $^{222}\text{Rn}_{\text{initial}}$ ) (Eq. (14)):

$$^{222}\text{Rn}_{\text{initial}} = ^{222}\text{Rn}_{\text{measured}} \exp(\lambda t_{\text{elapsed}}) \quad (14)$$

where  $^{222}\text{Rn}_{\text{measured}}$  is the measured radionuclide activity of the lagoon,  $t_{\text{elapsed}}$  is the time elapsed since the considered position

would have been reached by an earlier plume (i.e. 6 days, as a minimum value) and  $\lambda$  is radon decay constant.

The obtained initial activities range from  $66 \text{ Bq/m}^3$  (point 5, measured value of  $22 \text{ Bq/m}^3$ ) to  $129 \text{ Bq/m}^3$  (point 4, measured value of  $36 \text{ Bq/m}^3$ ), i.e. notably higher than the modeled range of values inside the plume. The discharge of the Rambla into the lagoon is therefore not sufficient to explain these high measured  $^{222}\text{Rn}$  activities. In addition, each measured value integrates both the "low" background activity of the lagoon and the "high" activity of the narrow plume of the Rambla. For a same sampling location, the modeled values are therefore comparatively overestimated.

Apart from the generalized  $^{222}\text{Rn}$  excess in the lagoon, point-sources  $^{222}\text{Rn}$  independent from the Rambla are highlighted around point 2, 4 and 5 (southern area) and points 1 and 3 (northern area). These sources are already taken into account in the balance based on activities extrapolated over the entire lagoon. Since no other surface water course than the Rambla del Albujón was found to carry water during any of the three sampling campaigns, these high- $^{222}\text{Rn}$  points cannot be explained by an additional river discharge. The southern point-source area was observed during each of the three campaigns, and has a considerable width (up to ten km). This temporal regularity, together with the spatial extension, suggests a quite large  $^{222}\text{Rn}$ -rich zone, possibly linked to a high hydraulic conductivity area or to the release of groundwater from agricultural drainage. By contrast, the northern  $^{222}\text{Rn}$  point source is narrower (covering one  $^{222}\text{Rn}$  measurement only, i.e. less than 1.5 km), and was not measured in July 2012. The temporal variability and tightness of this signal might thus be explained by a hidden and undocumented submarine emissary, like brine release, that discontinuously discharges high  $^{222}\text{Rn}$  in this area. Our knowledge of farmers' desalination practices is coherent with a higher rate of desalination in January than July.

In terms of global mass balance of the lagoon, the impact of such undocumented anthropogenic submarine water discharges is fortunately negligible (Fig. 5) in comparison to the total discharge from the Rambla. Regarding the other radionuclides ( $^{223}\text{Ra}$  and  $^{224}\text{Ra}$ ), it was not possible to evidence reliably any high activity point-source. This was caused mainly by the limited number of samples and by the lower spatial variability of measured activities.

## 6. Conclusion

This study is one of the first attempts to integrate radionuclide data ( $^{222}\text{Rn}$ ,  $^{224}\text{Ra}$ ,  $^{223}\text{Ra}$ ) in the hydrodynamic modeling of a lagoon. It also illustrates the importance of surface inputs on the calculation of radionuclide mass balances for SGD assessment. Indeed, surface water inputs from the only permanent stream, named Rambla, were shown to have a considerable impact on the lagoon radionuclide content. Very high radionuclide values along the coast, up to ten kilometers northwards and southwards from the outlet of the Rambla, were explained by the plume of the Rambla itself, overwhelming the possible contribution of other sources of radionuclides like SGD. As well, high nitrate levels along the western coast of Mar Menor were found to be mainly associated with the discharge of the Rambla, rather than due to high SGD areas. In addition to the baseflow activities issued from groundwater drainage, the Ra–Rn peaks measured in the Rambla were mostly due to the release of desalination brines from the Quaternary and deeper aquifers. High activities in the southern and northern coastal zone not reached by the plume evidenced the presence of significant radionuclide sources. Depending on the area, these high activities were explained by anthropogenic local releases of brines or by high hydraulic conductivity area and release of groundwater from agricultural drainage. Therefore, coupling radionuclide and modeling approaches helped avoiding severe misunderstanding regarding the SGD pattern.



The development of a site-specific approach for assessing the radionuclide activity of SGD demonstrated that the radionuclide signature of FSGD was better represented by porewater than by groundwater sampled from piezometers. It also showed that saline recirculation through the sediment cover was an important process. Yearly SGD fluxes of water calculated from the different tracers showed results ranging from  $0.4 \pm 0.3$  to  $2.2 \pm 0.5 \cdot 10^8 \text{ m}^3/\text{y}$  ( $^{222}\text{Rn}$ ),  $4.4 \pm 2.0$  to  $19 \pm 8 \cdot 10^8 \text{ m}^3/\text{y}$  ( $^{224}\text{Ra}$ ) for winter and summer, respectively, and  $1.3 \pm 0.6 \cdot 10^8 \text{ m}^3/\text{y}$  ( $^{223}\text{Ra}$ ) in winter. The seasonal variations could not be explained by high turbidity and the consequent increased diffusion from resuspended sediments, but were likely to reflect changes in meteoric conditions or bioirrigation fluxes. The impact of tidal pumping was evidenced as a driver for RSGD and the contribution of FSGD to the total SGD was assessed to range between 2% and 23%.

Finally, this study represents a notable step forward in the understanding of the water cycle of Mar Menor. Once overtaken the main methodological issues due to the high state of anthropization, it enabled the use of radionuclide mass balances, characterized the impact of surface water inputs and revealed that total SGD fluxes are much higher than initially expected from FSGD only. Therefore, it sets up a strong base to reliably focus further studies on specific environmental issues linked to SGD, like the quantification of inputs of nutrients through RSGD. Beyond the Mar Menor study, our methodology might be useful for many other sites by providing the criteria to decipher between natural processes and anthropogenic modifications.

## Acknowledgements

This work was developed within the scope of the Projects “Modelación Hidrológica en Zonas Semi Áridas” and “Monitorización Costera para el Mar Menor, CMS (463.01-08\_CLUSTER)” financed by the Regional Ministry of Universities, Business and Research (Region of Murcia, Spain). The authors acknowledge the Fundación Instituto Euromediterráneo del Agua (Murcia, Spain) for its fundamental financial support. Additional supports came through the “CARTAG-EAU” project financed by the French SICMED initiative the CGL2013-48424-C2-2-R project financed by the National Plan for Scientific and Technical Research and Innovation of Spain, and the 08225/PI/08 research project financed by “Programa de Generación del Conocimiento Científico de Excelencia” of the Fundación Seneca, Región de Murcia (II PCTRM 2007-10). AEMET, the Spanish agency of Meteorology, provided the atmospheric data for running the model.

## Appendix A. Supplementary material

Supplementary data associated with this article can be found, in the online version, at <http://dx.doi.org/10.1016/j.jhydrol.2015.03.015>.

## References

- Arévalo, L., 1988. El Mar Menor Como Sistema Forzado por el Mediterráneo. Control Hidráulico y Agentes Fuerza, vol. 5(1). Boletín del Instituto Español de Oceanografía, pp. 63–95.
- Baudron, P., Alonso-Sarria, F., García-Aróstegui, J.L., Cánovas-García, F., Martínez-Vicente, D., Moreno-Brotóns, J., 2013a. Identifying the origin of groundwater samples in a multi-layer aquifer system with random forest classification. *J. Hydrol.* 499, 303–315.
- Baudron, P., Barbecot, F., Gillon, M., García-Aróstegui, J.L., Travi, Y., Leduc, C., Gomariz Castillo, F., Martínez-Vicente, D., 2013b. Assessing groundwater residence time in a highly anthropized unconfined aquifer using bomb peak C-14 and reconstructed irrigation water H-3. *Radiocarbon* 55, 993–1006.
- Baudron, P., Barbecot, F., Aróstegui, J.L.G., Leduc, C., Travi, Y., Martínez-Vicente, D., 2014. Impacts of human activities on recharge in a multilayered semiarid aquifer (Campo de Cartagena, SE Spain). *Hydrol. Process.* 28, 2223–2236.
- Beck, A.J., Rapaglia, J.P., Cochran, J.K., Bokuniewicz, H.J., 2007. Radium mass-balance in Jamaica Bay, NY: evidence for a substantial flux of submarine groundwater. *Mar. Chem.* 106, 419–441.
- Beck, A.J., Rapaglia, J.P., Cochran, J.K., Bokuniewicz, H.J., Yang, S., 2008. Submarine groundwater discharge to Great South Bay, NY, estimated using Ra isotopes. *Mar. Chem.* 109, 279–291.
- Burnett, W.C., Cable, J.E., Corbett, D.R., 2003. Radon tracing of submarine groundwater discharge in coastal environments. In: Taniguchi, M., Wang, K., Gamo, T. (Eds.), *Land and Marine Hydrogeology*. Elsevier Publications, pp. 25–43.
- Burnett, W.C., Santos, I.C., Weinstein, Y., Swarzensky, P.W., Herut, B., 2007. Remaining uncertainties in the use of Rn-222 as a quantitative tracer of submarine groundwater discharge. In: *A New Focus on Groundwater–Seawater Interactions*, vol. 312. IAHS publ., Perugia, Italy, pp. 109–118.
- Burnett, W.C., Peterson, R., Moore, W.S., De Oliveira, J., 2008. Radon and radium isotopes as tracers of submarine groundwater discharge – results from the Ubatuba, Brazil SGD assessment intercomparison. *Estuar. Coast. Shelf Sci.* 76, 501–511.
- Cabezas, F., 2009. Balance hídrico del Mar Menor (Murcia). In: *El Mar Menor: Estado Actual Del Conocimiento Científico*. Publications of the IEA Foundation, Murcia, pp. 167–206.
- Cable, J.E., Burnett, W.C., Chanton, J.P., Weatherly, G.L., 1996. Estimating groundwater discharge into the northeastern Gulf of Mexico using radon-222. *Earth Planet. Sci. Lett.* 144, 591–604.
- Cockenpot, S., Claude, C., Radakovitch, O., 2015. Estimation of air–water gas exchange coefficient in a shallow lagoon based on  $^{222}\text{Rn}$  mass balance. *J. Environ. Radioactiv.* 143, 58–69.
- Cook, P.G., Wood, C., White, T., Simmons, C.T., Fass, T., Brunner, P., 2008. Groundwater inflow to a shallow, poorly-mixed wetland estimated from a mass balance of radon. *J. Hydrol.* 354, 213–226.
- Corbett, D.R., Burnett, W.C., Cable, P.H., Clark, S.B., 1998. A multiple approach to the determination of radon fluxes from sediments. *J. Radioanal. Nucl. Chem.* 236, 247–252.
- Cyronak, T., Santos, I.R., Erler, D.V., Eyre, B.D., 2013. Groundwater and porewater as major sources of alkalinity to a fringing coral reef lagoon (Muri Lagoon, Cook Islands). *Biogeosciences* 10, 2467–2480.
- Debreu, L., Marchesiello, P., Penven, P., Cambon, G., 2012. Two-way nesting in split-explicit ocean models: algorithms, implementation and validation. *Ocean Model* 49–50, 1–21.
- Dulaiova, H., Peterson, R., Burnett, W.C., Lane-Smith, D., 2005. A multi-detector continuous monitor for assessment of  $^{222}\text{Rn}$  in the coastal ocean. *J. Radioanal. Nucl. Chem.* 263 (2), 361–365.
- Dulaiova, H., Gonneea, M.E., Henderson, P.B., Charette, M.A., 2008. Geochemical and physical sources of radon variation in a subterranean estuary – implications for groundwater radon activities in submarine groundwater discharge studies. *Mar. Chem.* 110 (1–2), 120–127.
- Emery, W.J., Thomson, R.E., 2001. *Data Analysis Methods in Physical Oceanography*, second ed. Elsevier, Amsterdam, 639 pp.
- Ferrarin, C., Rapaglia, J., Zaggia, L., Umgieser, G., Zuppi, G.M., 2008. Coincident application of a mass balance of radium and a hydrodynamic model for the seasonal quantification of groundwater flux into the Venice Lagoon, Italy. *Mar. Chem.* 112, 179–188.
- García-Aróstegui, J.L., Jiménez-Martínez, J., Baudron, P., Martínez-Vicente, D.M., Guerra, J., 2012. Geometría del Campo de Cartagena e implicaciones en el funcionamiento hidrogeológico. In: *Nuevas Aportaciones Al Conocimiento De Los Acuíferos Costeros. Serie Hidrogeología y Aguas Subterráneas*. Instituto Geológico y Minero de España, Madrid, pp. 439–449.
- García-Orellana, J., Cochran, J.K., Bokuniewicz, H., Daniel, J.W.R., Rodellas, V., Heilbrun, C., 2014. Evaluation of  $^{224}\text{Ra}$  as a tracer for submarine groundwater discharge in Long Island Sound (NY). *Geochim. Cosmochim. Acta* 141, 314–330.
- García-Pintado, J., Martínez-Mena, M., Barberá, G.G., Albaladejo, J., Castillo, V.M., 2007. Anthropogenic nutrient sources and loads from a mediterranean catchment into a coastal lagoon: Mar Menor, Spain. *Sci. Total Environ.* 373, 220–239.
- García-Solsona, E., Masqué, P., García-Orellana, J., Rapaglia, J., Beck, A.J., Cochran, J.K., Bokuniewicz, H.J., Zaggia, L., Collavini, F., 2008. Estimating submarine groundwater discharge in the Isola La Cura, northern Venice Lagoon (Italy), by using the radium quartet. *Mar. Chem.* 109, 292–306.
- García-Solsona, E., García-Orellana, J., Masqué, P., Garcés, E., Radakovitch, O., Mayer, A., Estradé, S., Basterretxea, G., 2010. An assessment of karstic submarine groundwater and associated nutrient discharge to a mediterranean coastal area (Balearic Islands, Spain) using radium isotopes. *Biogeochemistry* 97, 211–229.
- Gattacceca, J.C., Mayer, A., Cucco, A., Claude, C., Radakovitch, O., Vallet-Coulomb, C., Hamelin, B., 2011. Submarine groundwater discharge in a subsiding coastal lowland: a  $^{226}\text{Ra}$  and  $^{222}\text{Rn}$  investigation in the Southern Venice lagoon. *Appl. Geochem.* 26, 907–920.
- Gonneea, M.E., Morris, P.J., Dulaiova, H., Charette, M.A., 2008. New perspectives on radium behavior within a subterranean estuary. *Mar. Chem.* 109, 250–267.
- IEA Foundation, 2011. *Modelación Hidrológica en Zonas Semiáridas – Subproject Modelización Hidrogeológica*. Final report. Fundación Instituto Euromediterráneo del Agua, Murcia, p. 470.
- Instituto Geológico y Minero de España (IGME), 1983. *Campaña de prospección geofísica en el Campo de Cartagena (Murcia). Sondeos Eléctricos Verticales. Technical report*. Madrid (Spain), Geological Survey of Spain, unpublished, 50pp.
- Jiménez-Martínez, J., Candela, L., García-Aróstegui, J.L., Aragón, R., 2012. A 3D geological model of Campo de Cartagena, SE Spain: hydrogeological implications. *Geol. Acta* 10, 49–62.

- Kluge, T., von Rohden, C., Sonntag, P., Lorenz, S., Wieser, M., Aeschbach-Hertig, W., Ilmberger, J., 2012. Localising and quantifying groundwater inflow into lakes using high-precision  $^{222}\text{Rn}$  profiles. *J. Hydrol.* 450–451, 70–81.
- Lefebvre, K., Barbecot, F., Ghaleb, B., Larocque, C., Gagné, S., 2013. Full range determination of  $^{222}\text{Rn}$  at the watershed scale by liquid scintillation counting. *Appl. Radiat. Isot.* 75, 71–76.
- Li, Y.-H., Gregory, S., 1974. Diffusion of ions in sea water and in deep-sea sediments. *Geochim. Cosmochim. Acta* 38, 703–714.
- Lillo Carpio, M., 1978. *Geomorfología litoral del Mar Menor*. Universidad de Murcia, vol. 8. *Papeles del Departamento de Geografía*, pp. 9–48.
- Lorenzen, G., Sprenger, C., Baudron, P., Gupta, D., Pekdeger, A., 2012. Origin and dynamics of groundwater salinity in the alluvial plains of western Delhi and adjacent territories of Haryana State, India. *Hydrol. Process.* 26, 2333–2345.
- Loveless, A.M., Oldham, C.E., Hancock, G.J., 2008. Radium isotopes reveal seasonal groundwater inputs to cockburn sound, a marine embayment in Western Australia. *J. Hydrol.* 351, 203–217.
- MacIntyre, S., Wanninkhof, R., Chanton, J.P., 1995. Trace gas exchange across the air–water interface in freshwater and coastal marine environments. In: Matson, P.A., Harris, R.C. (Eds.), *Biogenic Trace Gases: Measuring Emissions from Soil and Water*. Blackwell, Cambridge, Massachusetts, pp. 52–97.
- Martens, C., Kipphut, G., Klump, J., 1980. Sediment–water chemical exchange in the coastal zone traced by in situ radon-222 flux measurements. *Science* 208, 285–288.
- Martínez-Alvarez, V., Gallego-Elvira, B., Maestre-Valero, J.F., Tanguy, M., 2011. Simultaneous solution for water, heat and salt balances in a mediterranean coastal lagoon (Mar Menor, Spain). *Estuar. Coast. Shelf Sci.* 91, 250–261.
- McCoy, C.A., Corbett, D.R., Cable, J.E., Spruill, R.K., 2007. Hydrogeological characterization of southeast coastal plain aquifers and groundwater discharge to Onslow Bay, North Carolina (USA). *J. Hydrol.* 339, 159–171.
- Mejías, M., Ballesteros, B.J., Antón-Pacheco, C., Domínguez, J.A., García-Orellana, J., García-Solsona, E., Masqué, P., 2012. Methodological study of submarine groundwater discharge from a karstic aquifer in the Western Mediterranean Sea. *J. Hydrol.* 464–465, 27–40.
- Michael, H.A., Charette, M.A., Harvey, C.F., 2011. Patterns and variability of groundwater flow and radium activity at the coast: A case study from Waquoit Bay, Massachusetts. *Mar. Chem.* 127, 100–114.
- Moore, W.S., 1996. Large groundwater inputs to coastal waters revealed by  $^{226}\text{Ra}$  enrichments. *Nature* 380, 612–614.
- Moore, W.S., 2008. Fifteen years experience in measuring  $^{224}\text{Ra}$  and  $^{223}\text{Ra}$  by delayed-coincidence counting. *Mar. Chem.* 109, 188–197.
- Moore, W.S., Beck, M., Riedel, T., Rutgers van der Loeff, M., Dellwig, O., Shaw, T.J., Schetger, B., Brumsack, H.-J., 2011. Radium-based pore water fluxes of silica, alkalinity, manganese, DOC, and uranium: a decade of studies in the German Wadden Sea. *Geochim. Cosmochim. Acta* 75, 6535–6555.
- Mulligan, A.E., Charette, M.A., 2006. Intercomparison of submarine groundwater discharge estimates from a sandy unconfined aquifer. *J. Hydrol.* 327, 411–425.
- Peng, T.-H., Takahashi, T., Broecker, W., 1974. Surface radon measurements in the north Pacific station Papa. *J. Geophys. Res.* 79, 1772–1780.
- Pérez-Ruzafa, A., Fernández, A.I., Marcos, C., Gilabert, J., Quispe, J.I., García-Charton, J.A., 2005. Spatial and temporal variations of hydrological conditions, nutrients and chlorophyll a in a mediterranean coastal lagoon (Mar Menor, Spain). *Hydrobiologia* 550, 11–27.
- Perni, A., Martínez-Paz, J.M., 2013. A participatory approach for selecting cost-effective measures in the WFD context: the Mar Menor (SE Spain). *Sci. Total Environ.* 458–460, 303–311.
- Rapaglia, J., Ferrarin, C., Zaggia, L., Moore, W.S., Umgiesser, G., García-Solsona, E., García-Orellana, J., Masqué, P., 2010. Investigation of residence time and groundwater flux in Venice Lagoon: comparing radium isotope and hydrodynamical models. *J. Environ. Radioact.* 101, 571–581.
- Rodellas, V., García-Orellana, J., García-Solsona, E., Masqué, P., Domínguez, J.A., Ballesteros, B.J., Mejías, M., Zarroca, M., 2012. Quantifying groundwater discharge from different sources into a Mediterranean wetland by using  $^{222}\text{Rn}$  and Ra isotopes. *J. Hydrol.* 466–467, 11–22.
- Rodríguez Estrella, T., 2004. Decisive influence of neotectonics of the water connection between the Mediterranean Sea, Mar Menor and the Campo de Cartagena aquifers (South-East of Spain). In: *Groundwater and Saline Intrusion: Selected Papers from the 18th Salt Water Intrusion Meeting, 18 SWIM, Cartagena (Spain)*. IGME, Madrid.
- Santos, I.R., Eyre, B.D., 2011. Radon tracing of groundwater discharge into an Australian estuary surrounded by coastal acid sulphate soils. *J. Hydrol.* 396, 246–257.
- Santos, I.R., Niencheski, F., Burnett, W., Peterson, R., Chanton, J., Andrade, C.F.F., Milani, I.B., Schmidt, A., Knoeller, K., 2008. Tracing anthropogenically driven groundwater discharge into a coastal lagoon from southern Brazil. *J. Hydrol.* 353, 275–293.
- Santos, I.R., Burnett, W.C., Dittmar, T., Suryaputra, I.G.N.A., Chanton, J., 2009a. Tidal pumping drives nutrient and dissolved organic matter dynamics in a Gulf of Mexico subterranean estuary. *Geochim. Cosmochim. Acta* 73, 1325–1339.
- Santos, I.R., Dimova, N., Peterson, R.N., Mwashote, B., Chanton, J., Burnett, W.C., 2009b. Extended time series measurements of submarine groundwater discharge tracers ( $^{222}\text{Rn}$  and  $\text{CH}_4$ ) at a coastal site in Florida. *Mar. Chem.* 113, 137–147.
- Santos, I.R., Burnett, W.C., Chanton, J., Dimova, N., Peterson, R.N., 2009c. Land or ocean? Assessing the driving forces of submarine groundwater discharge at a coastal site in the Gulf of Mexico. *J. Geophys. Res.* 114, C04012.
- Santos, I.R., Eyre, B.D., Huettel, M., 2012. The driving forces of pore water and groundwater flow in permeable coastal sediments: a review. *Estuar. Coast. Shelf Sci.* 98, 1–15.
- Schiavo, M.A., Hauser, S., Povinec, P.P., 2009. Stable isotopes of water as a tool to study groundwater–seawater interactions in coastal south-eastern Sicily. *J. Hydrol.* 364, 40–49.
- Scholten, J.C., Pham, M.K., Blinova, O., Charrette, M.A., Dulaiova, H., Eriksson, M., 2010. Preparation of Mn-fiber standards for the efficiency calibration of the delayed coincidence counting system (RaDeCC). *Mar. Chem.* 121, 206–214.
- Schubert, M., Paschke, A., Lieberman, E., Burnett, W.C., 2012. Air–water partitioning of  $^{222}\text{Rn}$  and its dependence on water temperature and salinity. *Environ. Sci. Technol.* 46, 3905–3911.
- Senent, M., Martínez-Vicente, D., Cabezas, F., García-Aróstegui, J.L., Baudron, P., 2009. Aproximación mediante modelización matemática a la evaluación de las descargas del acuífero cuaternario del Campo de Cartagena al Mar Menor (Murcia). In: *El Mar Menor: Estado Actual Del Conocimiento Científico*. Murcia, pp. 109–130.
- Simonneau, J., 1973. *Mar Menor. Evolution sédimentologique et géochimique récente du remplissage*. Ph. D. Thesis. Paul Sabatier University. Toulouse.
- Smith, A.J., 2004. Mixed convection and density-dependent seawater circulation in coastal aquifers. *Water Resour. Res.* 40, W08309.
- Stieglitz, T., 2005. Submarine groundwater discharge into the near-shore zone of the Great Barrier Reef, Australia. *Mar. Pollut. Bull.* 51, 51–59.
- Stieglitz, T.C., Cook, P.G., Burnett, W.C., 2010. Inferring coastal processes from regional-scale mapping of  $^{222}\text{Rn}$  and salinity: examples from the Great Barrier Reef, Australia. *J. Environ. Radioact.* 101, 544–552.
- Stieglitz, T.C., Clark, J.F., Hancock, G.J., 2013. The mangrove pump: the tidal flushing of animal burrows in a tropical mangrove forest determined from radionuclide budgets. *Geochim. Cosmochim. Acta* 102, 12–22.
- Sun, Y., Torgersen, T., 1998. The effects of water content and Mn-fiber surface conditions on  $^{224}\text{Ra}$  measurement by  $^{220}\text{Rn}$  emanation. *Mar. Chem.* 62, 299–306.
- Taniguchi, M., Ishitobi, T., Shimada, J., 2006. Dynamics of submarine groundwater discharge and freshwater–seawater interface. *J. Geophys. Res.* 111, C01008.
- Teatini, P., Tosi, L., Viezzoli, A., Baradello, L., Zecchin, M., Silvestri, S., 2011. Understanding the hydrogeology of the Venice Lagoon subsurface with airborne electromagnetics. *J. Hydrol.* 411, 342–354.
- Turner, S.M., Malin, G., Nightingale, P.D., Liss, P.S., 1996. Seasonal variation of dimethyl sulphide in the North Sea and an assessment of fluxes to the atmosphere. *Mar. Chem.* 54, 245–262.
- Ullman, W., Aller, R., 1981. Diffusion coefficients in nearshore marine sediments. *Limnol. Oceanogr.* 27, 552–556.
- Velasco, J., Lloret, J., Millan, A., Marin, A., Barahona, J., Abellan, P., Sanchez-Fernandez, D., 2006. Nutrient and particulate inputs into the Mar Menor Lagoon (SE Spain) from an intensive agricultural watershed. *Water Air Soil Pollut.* 176, 37–56.
- Weinstein, Y., Burnett, W.C., Swarzenski, P.W., Shalem, Y., Yechieli, Y., Herut, B., 2007. Role of aquifer heterogeneity in fresh groundwater discharge and seawater recycling: an example from the Carmel coast, Israel. *J. Geophys. Res.* 112, C12016.



